Molecular Psychiatry (2021) 26:4066–4084
https://doi.org/10.1038/s41380-020-00958-2

ARTICLE

Valproate reverses mania-like behaviors in mice via preferential targeting of HDAC2

Ryan W. Logan[1] · Angela R. Ozburn[2,3] · Rachel N. Arey[4] · Kyle D. Ketchesin[1] · Alicia Winquist[5,6] · Andrew Crain[5,6] · Brian T. D. Tobe[5,6,7] · Darius Becker-Krail[1] · Matthew B. Jarpe[8] · Xiangning Xue[9] · Wei Zong[9] · Zhiguang Huo[10] · Puja K. Parekh[11] · Xiyu Zhu[1,12] · Ethan Fitzgerald[1] · Hui Zhang[1,13] · Jeffrey Oliver-Smith[1] · Lauren M. DePoy[1] · Mariah A. Hildebrand[1] · Evan Y. Snyder[5,6,14] · George C. Tseng[9,15] · Colleen A. McClung[1]

Received: 22 July 2020 / Revised: 20 October 2020 / Accepted: 6 November 2020 / Published online: 24 November 2020

Abstract

Valproate (VPA) has been used in the treatment of bipolar disorder since the 1990s. However, the therapeutic targets of VPA have remained elusive. Here we employ a preclinical model to identify the therapeutic targets of VPA. We find compounds that inhibit histone deacetylase proteins (HDACs) are effective in normalizing manic-like behavior, and that class I HDACs (e.g., HDAC1 and HDAC2) are most important in this response. Using an RNAi approach, we find that HDAC2, but not HDAC1, inhibition in the ventral tegmental area (VTA) is sufficient to normalize behavior. Furthermore, HDAC2 overexpression in the VTA prevents the actions of VPA. We used RNA sequencing in both mice and human induced pluripotent stem cells (iPSCs) derived from bipolar patients to further identify important molecular targets. Together, these studies identify HDAC2 and downstream targets for the development of novel therapeutics for bipolar mania.

Introduction

Valproate (VPA; also known as Depakote or generically as divalproex) is an antiepileptic drug that has been used in the United States as a treatment for the manic and mixed phases of bipolar disorder since its approval by the FDA in 1995

Supplementary information The online version of this article (https://doi.org/10.1038/s41380-020-00958-2) contains supplementary material, which is available to authorized users.

✉ Colleen A. McClung
mcclungca@upmc.edu

1 Translational Neuroscience Program, Department of Psychiatry, University of Pittsburgh School of Medicine, Pittsburgh, PA 15219, USA

2 Department of Behavioral Neuroscience, Portland Alcohol Research Center, Oregon Health & Science University, Portland, OR 97239, USA

3 VA Portland Health Care System, Portland, OR 97239, USA

4 Department of Molecular and Cellular Biology and Center for Precision Environmental Health, Baylor College of Medicine, Houston, TX 77030, USA

5 Sanford Burnham Prebys Medical Discovery Institute, La Jolla, CA 92037, USA

6 Sanford Consortium for Regenerative Medicine, La Jolla, CA 92037, USA

7 Department of Psychiatry, Veterans Administration Medical Center, La Jolla, CA 92037, USA

8 Regenacy Pharmaceuticals, 303 Wyman St, Suite 300, Waltham, MA 02451, USA

9 Department of Biostatistics, Graduate School of Public Health, University of Pittsburgh, Pittsburgh, PA 15261, USA

10 Department of Biostatistics, University of Florida, Gainesville, FL 32611, USA

11 Brain and Mind Research Institute, Department of Psychiatry, and Sackler Institute for Developmental Psychobiology, Weill Cornell Medicine, New York, NY 10021, USA

12 Department of Neuroscience, University of Pittsburgh, Pittsburgh, PA 15260, USA

13 Peking Union Medical College Hospital, 100730 Beijing, China

14 Department of Pediatrics, University of California San Diego, La Jolla, CA 92037, USA

15 Department of Computational and Systems Biology, University of Pittsburgh School of Medicine, Pittsburgh, PA 15213, USA

[1]. The anticonvulsant effects of VPA are thought to be due to the blockade of voltage-gated sodium channels and increased brain levels of gamma-aminobutyric acid (GABA) [2, 3]. However, the mechanisms that underlie the antimanic effects in bipolar disorder are less clear. In addition to the effects on GABAergic transmission, VPA is also a potent inhibitor of histone deacetylases (HDACs) at therapeutic serum levels (0.4–0.8 mM) [4, 5]. DNA is wrapped around histone proteins to form nucleosomes, allowing efficient DNA packaging into a chromatin structure. HDAC proteins remove acetyl groups from lysine residues on the tails of histone proteins, closing the chromatin and creating a less permissive state for transcription [6]. Inhibition of HDAC proteins generally leads to a more active chromatin structure and increased gene transcription at particular sites. The HDAC proteins fall into several classes based on sequence and cellular functions. Class I HDACs (HDAC1–3 and 8) are primarily nuclear proteins, while class II (a and b) HDACs (HDAC 4–7, 9, and 10) shuttle between the nucleus and cytoplasm [7]. The sirtuins are NAD+-dependent proteins that are considered class III HDACs [8]. HDAC11 is the only class IV HDAC [7]. In the adult mouse brain, class I HDACs are highly expressed with the exception of HDAC8. HDAC1 and HDAC2, in particular, may be differentially expressed in certain cell types and subregions of the brain [9]. Two members of class II HDACs (HDAC 4 and 5) are highly expressed in brain, while the others are expressed at much lower levels [7].

Inhibition of class I or II HDACs may protect neurons from oxidative stress-induced neuronal damage, which is frequently described in patients with bipolar disorder [10, 11]. Altered expression of class I HDACs has also been found in the hippocampus of postmortem brain from subjects with bipolar disorder [12]. Using in vivo imaging of HDAC-specific radiotracers in patients with bipolar disorder, altered levels and activity of HDACs were shown to be related to attention and emotion regulation, suggesting a role for HDACs in pathophysiology of bipolar disorder [13]. HDAC inhibitors have also been shown to reverse mania-like behaviors in rat models [14, 15], potentially via changes in growth factors and other factors related to neuronal and synaptic plasticity [11]. Therefore, it is possible that the antimanic and mood stabilizing effects of VPA are due to its properties as an HDAC inhibitor, particularly the inhibition of class I HDACs.

Our lab and others have utilized the *Clock*Δ19 mice for many years as an animal model to study human mania and the mechanisms that underlie current and potential mood stabilizing medications [16–22]. The CLOCK protein is a key component of the molecular transcriptional/translational feedback loop that controls circadian rhythms [23]. The *Clock*Δ19 mice have a point mutation, which creates a dominant-negative CLOCK protein [24]. These mice are hyperactive, display greater novelty seeking and risk taking behavior, have greater impulsivity, sleep less, have less behavioral despair, and have greater levels of reward seeking and motivation [16, 17, 20, 25–29]. Along with their behavioral phenotypes, the *Clock*Δ19 mice have increased dopaminergic activity (both firing and bursting) in the ventral tegmental area (VTA) [20, 30] that is largely responsible for their manic-like behaviors [27, 31, 32]. Multiple clinical studies have also suggested that alterations in dopamine neurotransmission in the VTA are central to bipolar mania [33–35]. Here, we use the *Clock*Δ19 mice to investigate the molecular mechanisms of action for VPA as an antimanic agent. Based on findings that highlight the possible role of class I HDACs in the pathophysiology of bipolar disorder and indications that VPA acts a potent HDAC inhibitor, we hypothesized that the therapeutic action of VPA for bipolar mania is, in part, via class I HDAC inhibition. In this study, we find that VPA treatment is able to normalize the behavioral phenotypes of the *Clock*Δ19 mice. We then employ a variety of pharmacological and genetic approaches to determine if inhibition of particular HDAC proteins may be responsible for the therapeutic actions of VPA. We investigate whether inhibition of HDACs specifically in the VTA is therapeutic and use RNA sequencing to help identify the molecular changes that occur in the VTA with HDAC inhibition. We extend our analyses into human induced pluripotent stem cells (iPSCs) derived from patients with bipolar disorder, and find a number of similar gene expression changes in response to treatment between mouse and human, which point toward potential molecular mechanisms of therapeutic action of VPA.

Results

VPA and suberoylanilide hydroxamic acid (SAHA) normalize behavior in the *Clock*Δ19 mice

Wild-type (Wt) and homozygous *Clock*Δ19 male and female mice were treated with vehicle or VPA compounded in the chow ad libitum [36]. Mice were then tested for the locomotor response to novelty, exploratory drive and avoidance behavior in the dark/light box and elevated plus maze (EPM), and behavioral despair in the forced swim test (FST). Consistent with previous studies [17, 19, 20, 26], male *Clock*Δ19 mice treated with vehicle were hyperactive in response to novelty, showed an increase in the time spent in the light of the dark/light box, increased time in the open arm in the EPM, and reduced immobility in the FST (Fig. 1A–D). These results were similar in female mice with the exception of the FST, where there were no differences between genotypes (Fig. 1I–L). In male mice, VPA treatment normalized time spent in the light in the dark/light

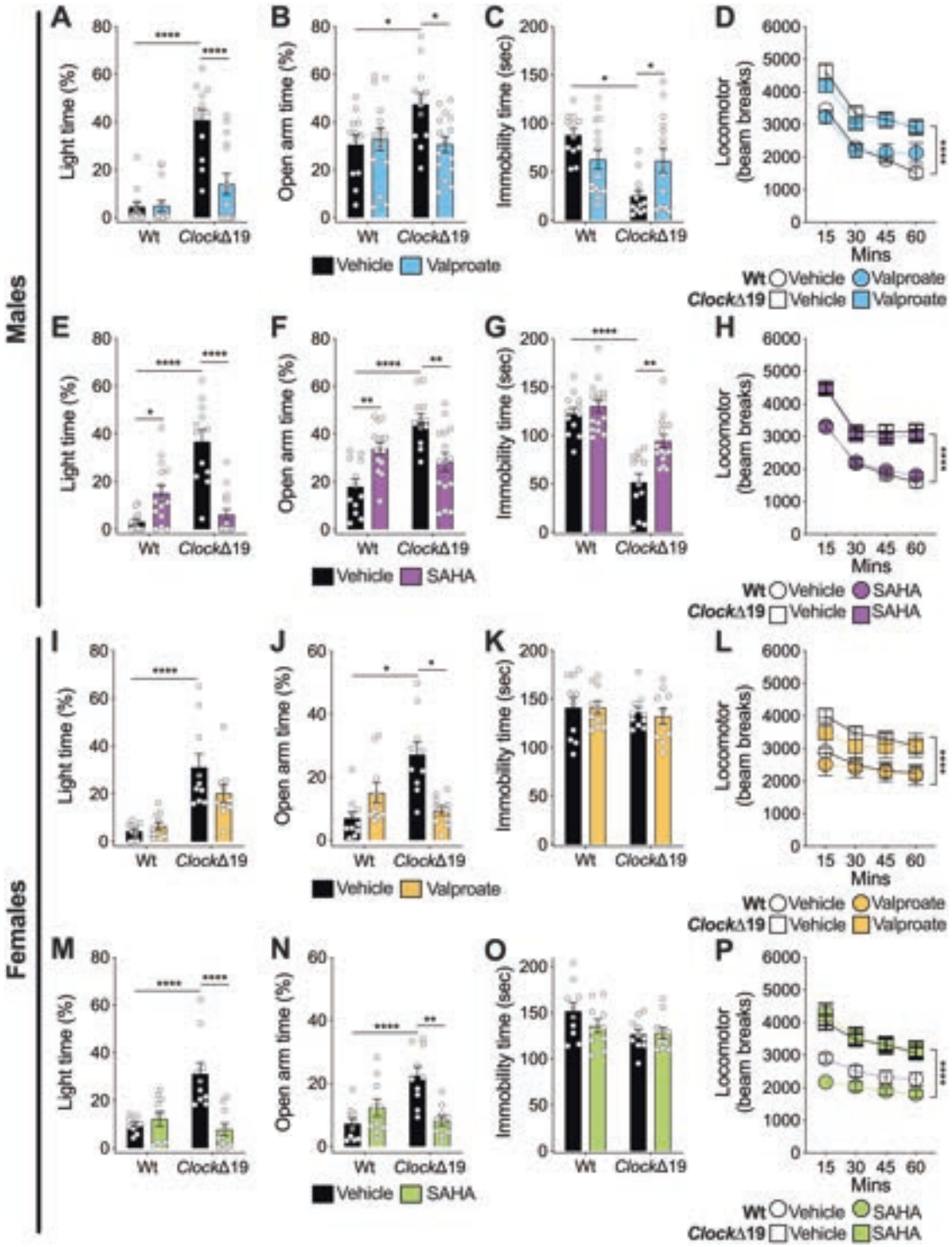

box, open arm time in the EPM, and immobility time in the FST (Fig. 1A–C). Interestingly, there was no effect of VPA on locomotor activity (Fig. 1D). In female *Clock*Δ19 mice, VPA had no significant effect on time in the light in the dark/light test (Fig. 1I), although VPA fully normalized open arm time in the EPM (Fig. 1J). VPA had no impact on the FST or locomotor activity in female mice (Fig. 1K, L). There were also no significant effects of VPA on Wt mice.

To determine if the effects of VPA could be recapitulated with an HDAC inhibitor, we administered the broad-spectrum inhibitor SAHA, which inhibits class I and class II HDACs. As expected, both VPA and SAHA increased histone H3 and H4 acetylation in both WT and *Clock*Δ19

◀ **Fig. 1 VPA and HDAC inhibition via SAHA reverse manic-like behaviors in *Clock*Δ19 mice.** Male (**A**–**D**) and female (**I**–**L**) Wt and *Clock*Δ19 mice were treated with VPA and tested for exploratory drive and avoidance behavior in the dark/light box (**A**, **I**) and EPM (**B**, **J**), behavioral despair in the FST (**C**, **K**), and locomotor response to novelty (**D**, **L**). Vehicle-treated male *Clock*Δ19 mice ($n = 12$) displayed increased time spent in the light side of the dark/light box (**A**), increased time in the open arm of the EPM (**B**), decreased immobility in the FST (**C**), and increased locomotor response to novelty (**D**) compared to Wt mice ($n = 12$). Treatment of male *Clock*Δ19 mice ($n = 15$) with VPA normalized time spent in the light side of the dark/light box (**A**), open arm time in the EPM (**B**), and immobility in the FST (**C**). However, VPA treatment had no effect on locomotor response to novelty (**D**). VPA treatment had no effect on male Wt mice ($n = 15$) (**A**–**D**). Vehicle-treated female *Clock*Δ19 mice ($n = 10$) also showed increased time spent in the light side of the dark/light box (**I**), increased time in the open arm of the EPM (**J**), and increased locomotor response to novelty (**L**), compared to Wt mice ($n = 10$). However, there was no genotype effect for immobility time in the FST (**K**). Treatment of female *Clock*Δ19 mice with VPA partially normalized time spent in the light side of the dark/light box (**I**) and normalized open arm time in the EPM (**J**), but had no effect on immobility time in the FST (**K**) and locomotor response to novelty (**L**). VPA treatment also had no effect on female Wt mice (**I**–**L**). Male (**E**–**H**) and female (**M**–**P**) Wt and *Clock*Δ19 mice were treated with SAHA and underwent the same behavioral testing as the VPA experiment, including dark/light box (**E**, **M**), EPM (**F**, **N**), FST (**G**, **O**), and locomotor response to novelty (**H**, **P**). Similar to the VPA experiment (**A**–**D**), vehicle-treated male *Clock*Δ19 mice showed increased time spent in the light side of the dark/light box (**E**), increased time in the open arm of the EPM (**F**), decreased immobility time in the FST (**G**), and increased locomotor response to novelty (**H**), compared to Wt mice. Treatment of male *Clock*Δ19 mice with SAHA normalized time spent in the light side of the dark/light box (**E**), open arm time in the EPM (**F**), and immobility in the FST (**G**), with no effect on locomotor response to novelty (**H**). SAHA-treated Wt mice also showed an increase in time in the light side of the dark/light box (**E**) and an increase in time in the open arm of the EPM (**F**). Similar to the VPA experiment (**I**–**L**), vehicle-treated female *Clock*Δ19 mice also showed increased time spent in the light side of the dark/light box (**M**), increased time in the open arm of the EPM (**N**), and increased locomotor response to novelty (**P**), with no effect on immobility time in the FST (**O**). Treatment of female *Clock*Δ19 mice with SAHA normalized time spent in the light side of the dark/light box (**M**) and open arm time in the EPM (**N**), with no effect on immobility time in the FST (**O**) or locomotor response to novelty (**P**). SAHA treatment had no effect on female Wt mice (**M**–**P**). Data are represented as mean ± SEM. Data in (**A**–**C**, **E**–**G**, **I**–**K**, **M**–**O**) were analyzed using two-way ANOVA followed by Tukey's post hoc tests if significant interaction. Data in (**D**, **H**, **L**, **P**) were analyzed using two-way repeated measures ANOVA. $*p < 0.05$; $**p < 0.01$; $****p < 0.0001$, with lines between bars representing significant differences between those groups.

mice (Supplementary Fig. 1). Similar to VPA, in male *Clock*Δ19 mice, SAHA normalized time in the light in the dark/light test, open arm time in the EPM, and immobility in the FST with no difference in locomotor activity (Fig. 1E–H). Interestingly, in Wt male mice there was an increase in time in the light in the dark/light box and increased open arm time in the EPM, suggesting an anxiolytic effect in Wt mice (Fig. 1E–H). Female *Clock*Δ19 mice had similar behavioral responses to the male mice in the dark/light box and EPM in response to SAHA with no change in the FST or in locomotor activity (Fig. 1M–P). Wt female mice had no significant response to SAHA. Taken together, these data show that VPA generally normalizes the manic-like behavior of the *Clock*Δ19 mice, and these results can be mimicked using an HDAC inhibitor.

The class I HDAC inhibitor MS275 normalizes manic-like behavior in the *Clock*Δ19 mice

To begin to determine the specific classes of HDAC inhibitors that are able to normalize manic-like behavior in the *Clock*Δ19 mice, we tested MS275, a specific inhibitor of class I HDACs, and MC1568, a specific inhibitor of class IIa HDACs (Fig. 2). Male and female Wt and *Clock*Δ19 mice were treated with vehicle or 20 mg/kg of MS275 [37] or MC1568 [38]. In male *Clock*Δ19 mice, MS275 reduced light time in the light/dark box, reduced center time in the open field, reduced latency to immobility in the FST (Fig. 2A, C, D). There were no significant changes in EPM behavior (Fig. 2B) and locomotor activity (Fig. 2F). In female *Clock*Δ19 mice, there was an overall genotype effect in open arm time in the EPM with no significant interactions with treatment (Fig. 2G). In contrast, MC1568 and MS275 significantly reduced open arm time in the EPM (Fig. 2H). Only MS275 reduced center time in the open field of female *Clock*Δ19 mice (Fig. 2I). Neither MC1568 nor MS275 had significant effects on latency to immobility (Fig. 2J) and immobility time (Fig. 2K) in the FST. There were treatment differences in locomotor activity (Fig. 2L). The only significant effect in Wt mice was an increase in open arm time in the EPM with both MS275 and MC1568 treatment (Fig. 2H). Overall, MC1568 had inconsistent effects on behavior in *Clock*Δ19 mice compared to MS275. These results suggest that class I HDAC inhibition generally reverses manic-like behavior with more selective effects of class IIa HDAC inhibition on these behaviors.

An inhibitor of HDAC1 and 2, ACY957, normalizes manic-like behavior in the *Clock*Δ19 mice

ACY957 is a potent inhibitor of HDAC1 and HDAC2 (IC50 of 7 and 18 mM) with very limited activity against HDAC3 (IC50 = 1300 nM) and no activity against HDACs 4–8. Therefore, we used ACY957 to further define the particular HDAC proteins in which inhibition leads to reversal of manic-like behaviors in the *Clock*Δ19 mice (Fig. 3). Wt and *Clock*Δ19 male and female mice were treated with 10 mg/kg of ACY957, based on our HPLC measurement of plasma levels and high brain penetrance following i.p. administration in Wt and *Clock*Δ19 mice (Supplementary Fig. 2A, B). We found maximal

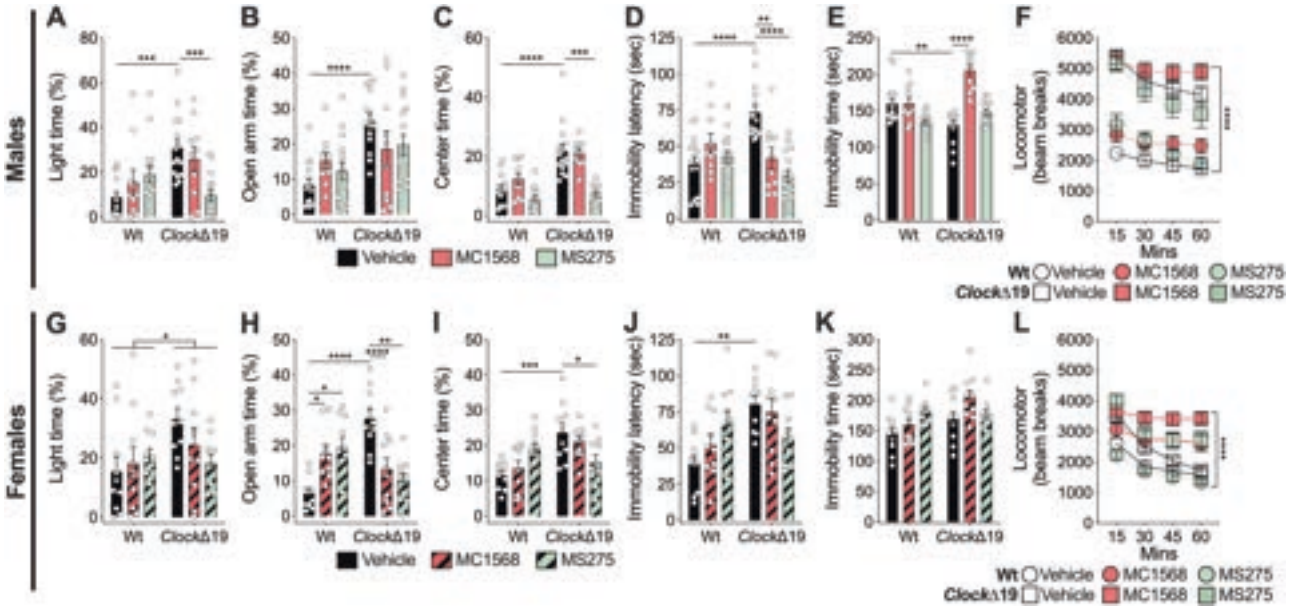

Fig. 2 Class I HDAC inhibition via MS275 normalizes manic-like behavior in *Clock*Δ19 mice. Male (**A**–**F**) and female (**G**–**L**) Wt and *Clock*Δ19 mice were treated with the Class I HDAC inhibitor, MS275 ($n = 15$ male; $n = 10$ female), or the class IIa HDAC inhibitor, MC1568 ($n = 10$ male; $n = 10$ female), and tested for exploratory drive and avoidance behavior in the dark/light box (**A**, **G**), EPM (**B**, **H**), and open field test (**C**, **I**), behavior despair in the FST (**D**, **E**, **J**, **K**), and locomotor response to novelty (**F**, **L**). Vehicle-treated male *Clock*Δ19 mice ($n = 15$) showed increased time in the light side of the dark/light box (**A**), increased time in the open arm of the EPM (**B**), increased center time in the open field (**C**), increased latency to immobility (**D**) and decreased immobility time in the FST (**E**), and increased locomotor response to novelty (**F**) compared to Wt mice ($n = 15$). Treatment of male *Clock*Δ19 mice with MS275 normalized time spent in the light side of the dark/light box (**A**), center time in the open field test (**C**), and latency to immobility in the FST (**D**). There were no effects in the EPM (**B**), in the FST (**E**), or locomotor response to novelty (**F**). Treatment of male *Clock*Δ19 mice with MC1568 normalized latency to immobility (**D**) and immobility time (**E**) in the FST, with no effect on time spent in the light side of the dark/light box (**A**), open arm time in the EPM (**B**), center time in the open field (**C**), or locomotor response to novelty (**F**). MS275 and MC1568 both had no effect on male Wt mice (**A**–**F**). Vehicle-treated female *Clock*Δ19 mice ($n = 10$) showed increased time spent on the light side of the dark/light box (**G**), increased time in the open arm of the EPM (**H**), increased center time in the open field (**I**), increased latency to immobility in the FST (**J**), and increased locomotor response to novelty (**L**), with no effect on immobility time in the FST (**K**). Treatment of female *Clock*Δ19 mice with MS275 normalized open arm time in the EPM (**H**) and center time in the open field (**I**). There was no effect in the dark/light box (**G**) and on the latency to immobility in the FST (**J**), with no effect on immobility time in the FST (**K**) or locomotor response to novelty (**L**). Treatment of female *Clock*Δ19 mice with MC1568 normalized open arm time in the EPM (**H**), with no effects on time spent in the light side of the dark/light box (**G**), center time in the open field test (**I**), latency to immobility in the FST (**J**), immobility time in the FST (**K**), or locomotor response to novelty (**L**). Both MS275 and MC1568 treatment increased time spent in the open arm of the EPM in Wt mice (**H**). Data are represented as mean ± SEM. Data in (**A**–**E**, **G**–**K**) were analyzed using two-way ANOVA followed by Tukey's post hoc tests if significant interaction. Data in (**F**, **L**) were analyzed using two-way repeated measures ANOVA. $^{*}p < 0.05$; $^{**}p < 0.01$; $^{***}p < 0.001$; $^{****}p < 0.0001$, with lines between bars representing significant differences between those groups.

concentrations at 1 h post injection, which were maintained at physiologically relevant levels for at least 4 h (Supplementary Fig. 2A, B). In response to ACY957, we found that in male *Clock*Δ19 mice, ACY957 reduced time in the light in the dark/light box, reduced open arm time in the EPM, decreased latency to immobility in the FST, and increased immobility time in the FST (Fig. 3A, B, D, E). There was no effect in the open field or on locomotor activity (Fig. 3C, F). In female *Clock*Δ19 mice, ACY957 decreased open arm time in the EPM with no effect in any other measure (Fig. 3G–L). In male Wt mice, ACY957 had mostly the opposite effect seen in *Clock*Δ19 mice with increased time in the light in the dark/light box, increased open arm time in the EPM, increased latency to immobility in the FST, and decreased immobility time (Fig. 3A, B, D, E). In female Wt mice, there was also an increase in open arm time in the EPM (Fig. 3H). These data suggest inhibition of HDAC1 and 2 had a particularly strong effect on male mice with a normalization of manic-like behavior in the *Clock*Δ19 mice and opposing effects in Wt mice. These sex-specific effects of ACY957 on behavior were independent of plasma and brain levels (Supplementary Fig. 2). We also measured body weights and found that as expected *Clock*Δ19 mice were heavier than Wt mice at baseline, and ACY957 treatment slightly reduced body weight in the *Clock*Δ19 males and females, with no change in Wt mice, suggesting overall health was not impacted (Supplementary Fig. 2C, D).

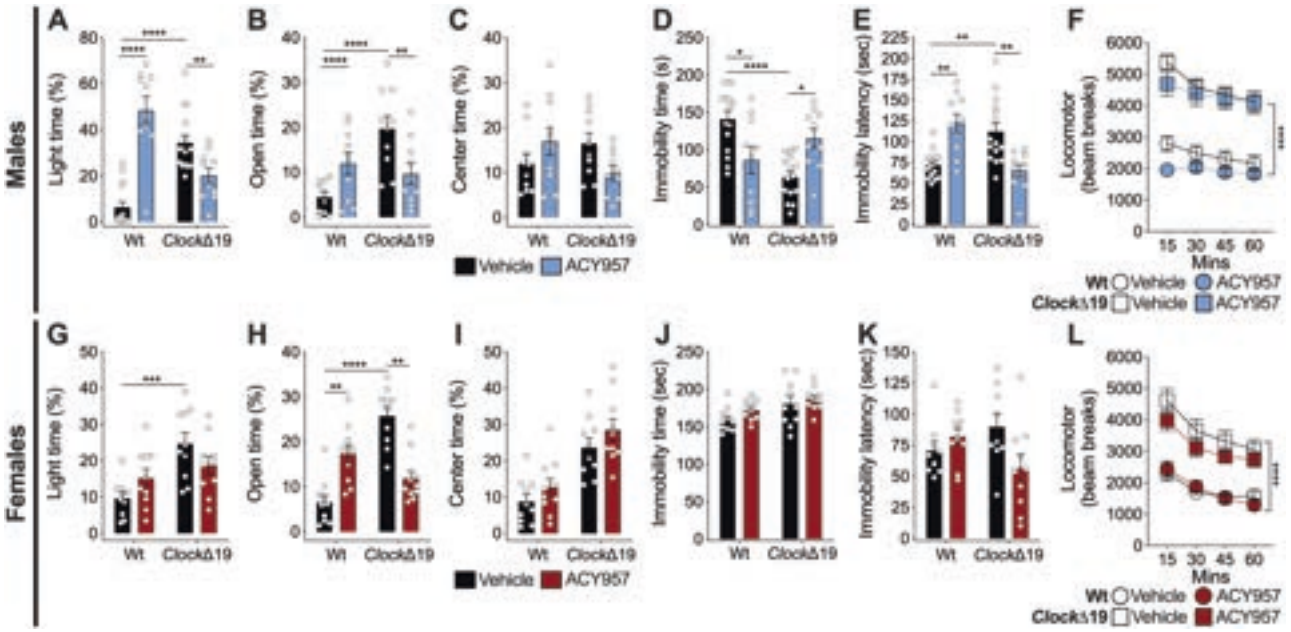

Fig. 3 Inhibition of HDAC1 and 2 via ACY957 normalizes manic-like behavior in *Clock*Δ19 mice. Male (**A**–**F**) and female (**G**–**L**) Wt and *Clock*Δ19 mice were treated with ACY957 ($n = 15$ male; $n = 10$ female) and tested for exploratory drive and avoidance behavior in the dark/light box (**A**, **G**), EPM (**B**, **H**), and open field test (**C**, **I**), behavioral despair in the FST (**D**, **E**, **J**, **K**), and locomotor response to novelty (**F**, **L**). Vehicle-treated male *Clock*Δ19 mice showed increased time in the light side of the dark/light box (**A**), increased time in the open arm of the EPM (**B**), decreased immobility time (**D**) and increased latency to immobility (**E**) in the FST, and increased locomotor response to novelty (**F**), with no effect on center time in the open field (**C**). Treatment of male *Clock*Δ19 mice with ACY957 normalized time spent in the light side of the dark/light box (**A**), open arm time in the EPM (**B**), immobility time (**D**) and latency to immobility (**E**) in the FST, with no effect on center time in the open field test (**C**) or locomotor response to novelty (**F**). In male Wt mice, ACY957 increased time in the light side of the dark/light box (**A**), increased open arm time in the EPM (**B**), and decreased immobility time (**D**) and increased latency to immobility (**E**) in the FST. Vehicle-treated female *Clock*Δ19 mice showed increased time in the light side of the dark/light box (**G**), increased time in the open arm of the EPM (**H**), and increased locomotor response to novelty (**L**), with no effect on center time in the open field test (**I**), immobility time (**J**), or latency to immobility (**K**) in the FST. Treatment of female *Clock*Δ19 mice with ACY957 normalized open arm time in the EPM (**H**) but had no effect on any of the other behavioral measures (**G**, **I**–**L**). In female Wt mice, ACY957 increased time spent in the open arm in the EPM (**H**). Data are represented as mean ± SEM. Data in (**A**–**E**, **G**–**K**) were analyzed using two-way ANOVA followed by Tukey's post hoc tests if significant interaction. Data in (**F**, **L**) were analyzed using two-way repeated measures ANOVA. $*p < 0.05$; $**p < 0.01$; $***p < 0.001$; $****p < 0.0001$, with lines between bars representing significant differences between those groups.

Knockdown of HDAC2, but not HDAC1, in the VTA normalizes manic-like behavior in the *Clock*Δ19 mice

Following the positive results with the HDAC1 and 2 inhibitors, ACY957, we aimed to determine if there are differences in *Hdac1* or *Hdac2* expression in the *Clock*Δ19 mice in the VTA and how this was changed following ACY957 treatment (Fig. 4). We chose the VTA based on our previous studies, which found that *Clock*Δ19 mice have increased firing and bursting of VTA dopamine neurons relative to Wt mice and this abnormal activity seems to underlie many of their behavioral phenotypes [16, 19, 20, 31, 39]. We found no differences across groups in *Hdac1* expression (Fig. 4A). However, we found ACY957 significantly reduced the expression of *Hdac2* in the VTA of both Wt and *Clock*Δ19 mice (Fig. 4A). There were no differences in the expression of these HDACs in the VTA between Wt and *Clock*Δ19 mice at baseline. We then decided to take a molecular approach to knockdown expression of each HDAC specifically in the VTA. To do this, we created a short hairpin RNA (shRNA) sequence directed specifically toward *Hdac1* or *Hdac2* (Fig. 4B, C and Supplementary Fig. 3). We focused on male mice here as they had a more robust overall behavioral response to the pharmacological compounds tested. We found that in the *Clock*Δ19, mice knockdown of HDAC2, but not HDAC1, led to the normalization of time spent in the light side of the dark/light box, time in the open arm of the EPM, and time in the center of the open field (Fig. 4D–F). In addition, HDAC2 knockdown increased immobility time in the FST and decreased the latency to immobility (Fig. 4G–H). There was no impact on locomotor activity (Fig. 4I). In contrast, HDAC1 and HDAC2 knockdown led to increased time in the open arms of the EPM in Wt mice (Fig. 4E), and HDAC2 knockdown reduced immobility

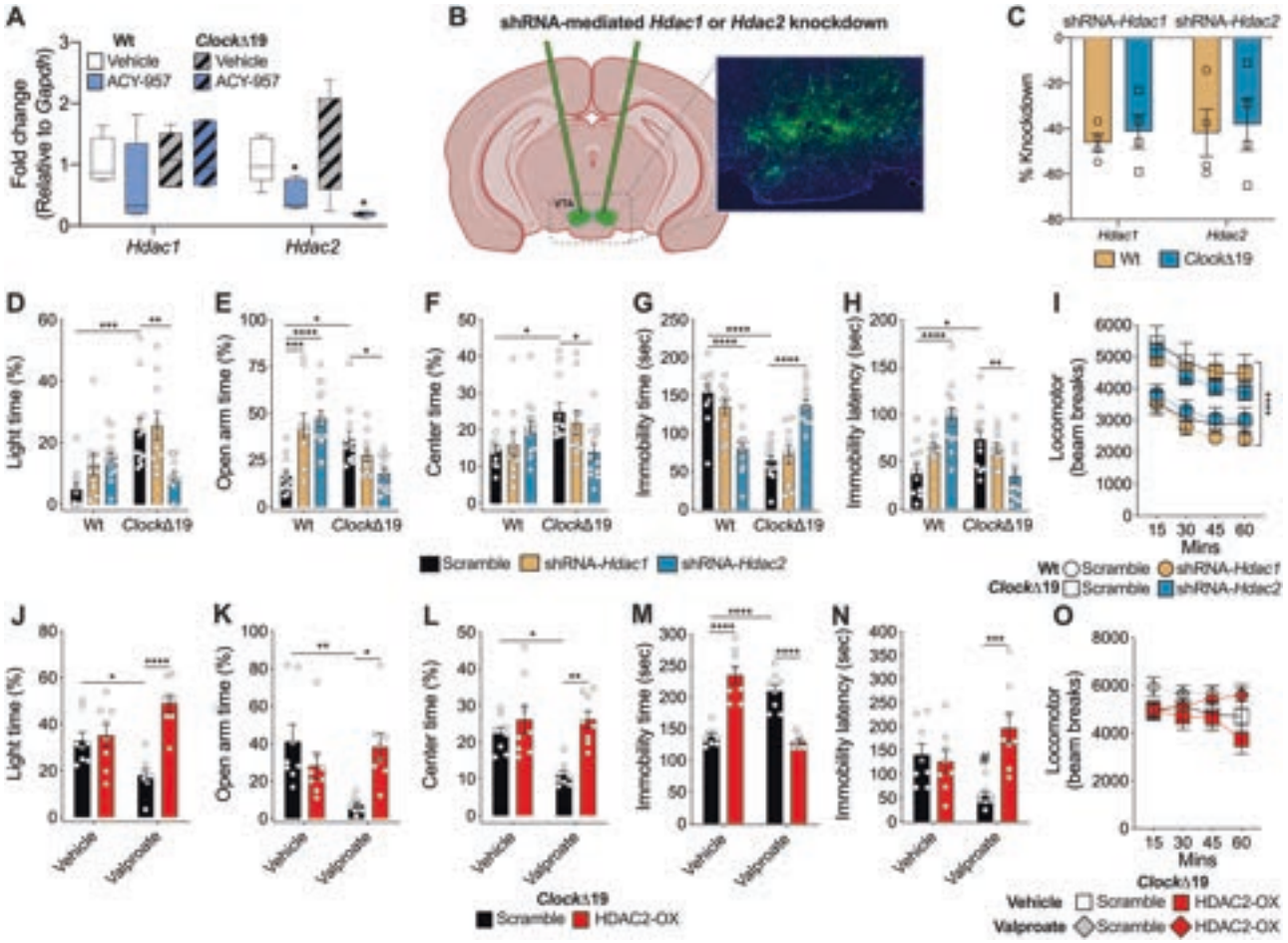

Fig. 4 Knockdown of HDAC2, but not HDAC1, in the VTA normalizes manic-like behavior in *Clock*Δ19 mice. There was a significant reduction of mRNA expression of *Hdac2* in the VTA in both Wt and *Clock*Δ19 mice following treatment with ACY957. Two-way ANOVA, $*p < 0.05$ main effect of treatment (**A**). No differences in *Hdac1* expression were observed following ACY957 treatment (**A**). Male Wt and *Clock*Δ19 mice ($n = 4$ per genotype per condition) were injected into the VTA with shRNA-*Hdac1* or shRNA-*Hdac2* to site specifically knockdown *Hdac1* or *Hdac2* in the VTA (**B**). Percent knockdown of *Hdac1* and *Hdac2* following viral injections is shown in (**C**). Scramble shRNA-injected male *Clock*Δ19 mice showed increased time in the light side of the dark/light box (**D**), increased time in the open arm of the open field test (**E**), increased center time in the open field test (**F**), decreased immobility time (**G**) and increased latency to immobility (**H**) in the FST, and increased locomotor response to novelty (**I**). shRNA-mediated knockdown of *Hdac2*, but not *Hdac1*, normalized time spent in the light side of the dark/light box (**D**), time spent in the open arm in the EPM (**E**), time spent in the center of the open field test (**F**), and immobility time (**G**) and latency to immobility (**H**) in the FST, with no effect on locomotor response to novelty (**I**). In contrast, shRNA-mediated knockdown of *Hdac1* and *Hdac2* in Wt mice increased time spent in the open arm of the open field test (**E**), and knockdown of *Hdac2* reduced immobility time (**G**) and increased latency to immobility in FST (**H**). Treatment of male GFP-only *Clock*Δ19 mice with VPA normalizes time spent in the light side of the dark/light box (**J**), open arm time in the EPM (**K**), center time in the open field test (**L**), on immobility time (**M**) and latency to immobility (**N**) in the FST, with no effects on locomotor response to novelty (**O**). VPA treatment of mice with *Hdac2* overexpression in the VTA had no effect on any of the behavioral measures (**J**–**L**, **N**, **O**), except for significantly increasing immobility time in the FST (**M**). Scramble Wt and *Clock*Δ19 male mice, $n = 12$; shRNA-*Hdac1* Wt and *Clock*Δ19 male mice, $n = 10$; and shRNA-*Hdac2* Wt, $n = 15$, and *Clock*Δ19 male mice, $n = 12$. Overexpression of *Hdac2* or control GFP, $n = 8$ per vehicle or VPA treatment. Data are represented as mean ± SEM. Data in (**D**–**H**, **J**–**N**) were analyzed using two-way ANOVA followed by Tukey's post hoc tests if significant interaction. Data in (**I**, **O**) were analyzed using two-way repeated measures ANOVA. $*p < 0.05$; $**p < 0.01$; $***p < 0.001$; $****p < 0.0001$, with lines between bars representing significant differences between those groups.

time in the FST and increased latency to immobility in these mice (Fig. 4G–H). There were no effects on other behavioral tests. Importantly, these data demonstrate that the knockdown of *Hdac2*, but not *Hdac1*, in the VTA is sufficient to normalize manic-like behavior in *Clock*Δ19 male mice.

HDAC2 inhibition in the VTA is necessary for the normalization of manic-like behavior by VPA in *Clock*Δ19 mice

To determine if a reduction in HDAC2 in the VTA was necessary for the therapeutic-like effects of VPA, we

utilized a viral approach to overexpress HDAC2 in the VTA of *Clock*Δ19 mice (Fig. 4J–O). Importantly, we found that while VPA treatment in *Clock*Δ19 mice with the scramble shRNA in the VTA normalized behavior in the dark/light box, EPM, open field, and FST as found previously (Fig. 1), mice with HDAC2 overexpression in the VTA showed no effect of VPA treatment on any of these behavioral tests (Fig. 4J–O). Thus, taken together HDAC2 inhibition was both necessary and sufficient for the therapeutic effects of VPA in these behavioral measures.

VPA and ACY957 lead to common gene expression changes in the VTA of *Clock*Δ19 male mice

To determine the gene expression changes that underlie the behavioral response to VPA and the more specific HDAC inhibitor, ACY957, we performed RNA sequencing of VTA tissue in Wt and *Clock*Δ19 male mice treated for 14 days with VPA (20 g/kg compounded in chow), ACY957 (10 mg/kg), or vehicle (Fig. 5). Tissue was collected 24 h following the final dose. We identified 234 differentially expressed (DE) transcripts (111 upregulated) with VPA treatment (Supplementary Data 1 and 2) and 540 DE transcripts (315 upregulated) with ACY957 (Supplementary Data 3 and 4). Enrichment analysis of the top pathways regulated by both VPA and ACY957 included peptide ligand-binding receptors (e.g., *Nmu, Nmur2, Edn1*, and *Edn2*) and serine-type endopeptidase inhibitor activity (e.g., *Serping1, Serpinh1, Serpind1, Papln*, and *A2m*) (Fig. 5A). The top pathways enriched in VPA-treated *Clock*Δ19 mice included cellular response to interferon-gamma and GABA synthesis, release, reuptake, and degradation (Fig. 5A). The top pathways regulated by ACY957 were related to neuregulin binding, inflammatory processes, growth factor binding, and extracellular matrix organization (Fig. 5A). We also identified MSX2, a transcriptional repressor that is highly expressed in DA midbrain neurons, as a potential upstream regulator for VPA DE transcripts (Fig. 5A) [40]. There were also a number of potential upstream regulators identified for ACY, including several circadian transcription factors (e.g., ARNTL and CLOCK) and factors within canonical NF-κB signaling pathways, including RELA and NFKB1 (Fig. 5A). There were only 24 transcripts differentially expressed in both VPA and ACY957 treatments, including several circadian genes, which have been associated with bipolar disorder, *Nmur2* [41] and *Rorc* [42] (Fig. 5A).

To identify gene co-expression networks associated with treatment response in mania-like behaviors, we used weighted gene co-expression network analysis (WGCNA) to build gene modules on *Clock*Δ19 mice. Module preservation analysis was performed to identify highly robust modules [43]. We identified 19 modules that survived preservation analysis (Fig. 5B). Given our focus on effects of treatment in *Clock*Δ19 mice, we used module differential connectivity (MCD) analysis to determine whether module connectivity increased or decreased by treatment condition, VPA or ACY957. If a module gains connectivity, this indicated that there was more coordinated expression within the module in VPA or ACY957 compared to vehicle controls, while a module that lost connectivity indicated that co-expression was more coordinated in control mice. The pie chart summarizes the results for the MDC analysis with only one module gained and lost (Fig. 5B). The black and brown modules were particularly interesting, as these modules were the only modules that were significantly changed in *Clock*Δ19 mice treated with VPA or ACY957 and showed significant enrichment of DE transcripts in *Clock*Δ19 mice (Fig. 5B).

Subsequent analyses focused on the brown module as the only module that was significantly gained in *Clock*Δ19 mice and also had significant DE enrichment for both VPA and ACY957. We highlighted hub genes based on their high level of co-expression and the assumption that these genes are predicted to control the expression of other transcripts in the module. In the brown module, there were 27 DE transcripts for only VPA and one transcript for ACY957, with only three transcripts (*Fbxo32, Bcas1*, and *Kcnk13*) that were differentially expressed in both VPA and ACY957 cohorts of *Clock*Δ19 mice (Fig. 5C). The hub genes, *Fbxo32, Bcas1*, and *Kcnk13* were of the 24 shared DE transcripts and may represent key targets for therapeutic action of both VPA and ACY957 via HDAC inhibition.

Highly overlapping transcriptional profiles between *Clock*Δ19 mice and iPS cells from bipolar subjects treated with VPA and ACY957

In patients with bipolar mania, VPA is often used following ineffective treatment rounds with lithium. iPSCs derived from patients who do or do not respond to lithium (i.e., lithium responders versus nonresponders) have different molecular, cellular, and physiological phenotypes in response to lithium and other therapeutics [44–46]. Therefore, we used iPSCs derived from lithium nonresponders (Supplementary Table 1) as an approach to gain insight into the therapeutic mechanisms unique to VPA. Meta-analysis was conducted on DE transcripts from two patients (two to three clones per patient and two to four replicates per sample; Supplementary Data 5 and 6). We found minimal alterations in gene markers of major cell types across treatment conditions (Supplementary Table 2), similar to our previous work [46]. We identified 2325 and 1647 DE transcripts ($p < 0.05$) in VPA- and ACY957-treated iPSCs, respectively (Fig. 5D, E), with 958 transcripts shared

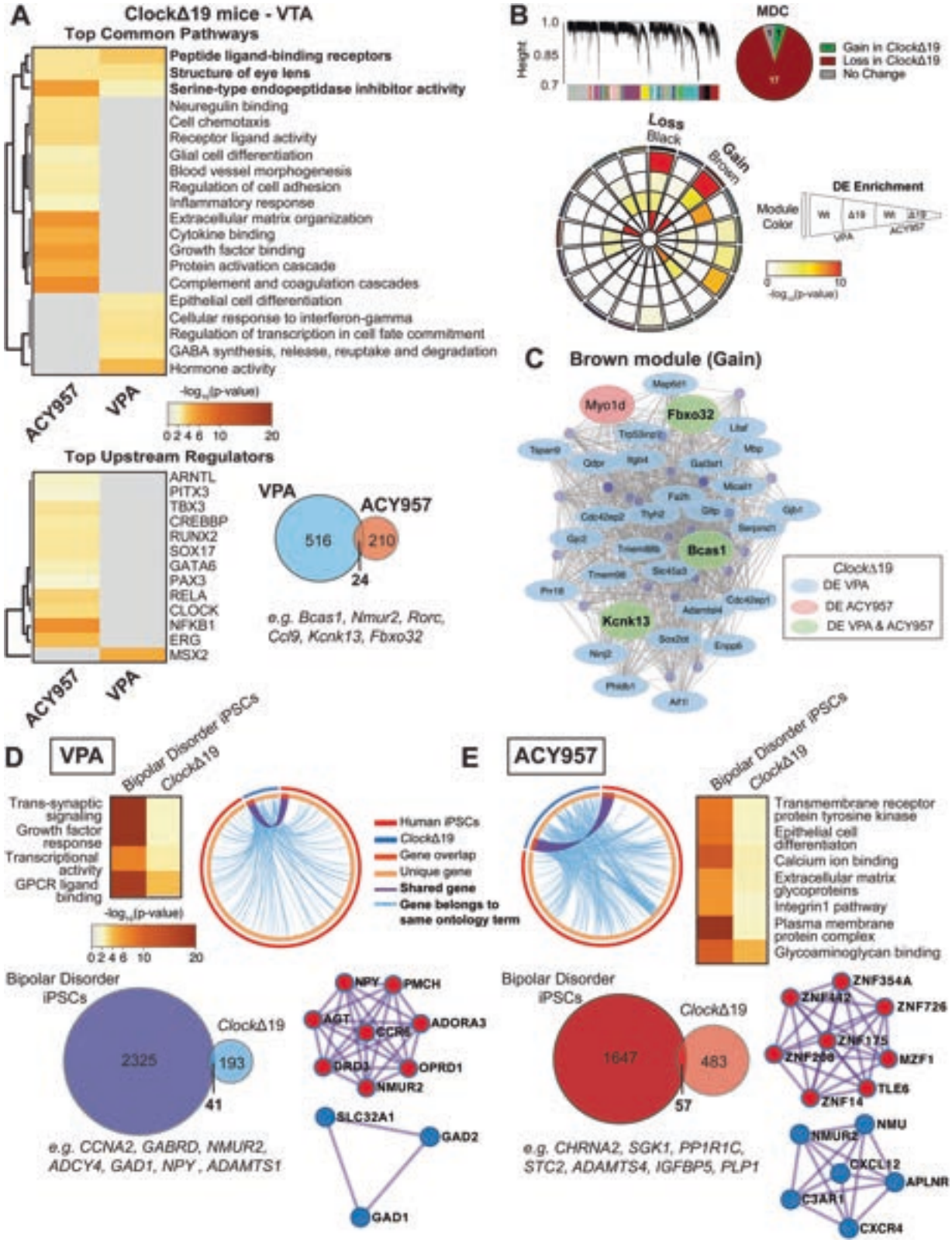

between treatments (Supplementary Fig. 4A, B). Metascape analysis [47] revealed that many of these transcripts were highly shared across similar pathways and also revealed common upstream regulators (Supplementary Fig. 4A, C). To identify pathways that were common between human and mouse, separate enrichment analyses were conducted

◀ **Fig. 5 The effects of VPA and ACY957 on the VTA transcriptome of *Clock*Δ19 mutant mice and patient-derived human iPSCs.** Top pathways and upstream regulators enriched in *Clock*Δ19 mutant mice treated with either VPA or the class I HDAC inhibitor, ACY957 (**A**). Overlap of top differentially expressed (DE) transcripts in *Clock*Δ19 mutant mice treated with VPA relative to ACY957 (**A**) and the top upstream regulators enriched from the 24 DE transcripts similarly altered by VPA and ACY957 ($p < 0.05$ and logFC ≤ −0.26 and ≥0.26). Weighted gene co-expression network analysis (WGCNA) was used to generate co-expression modules, with the network structure built on all samples from wild-type (Wt) and *Clock*Δ19 mutant mice (**B**). The 19 modules that survived module preservation analysis were assigned colors and the dendrogram depicts the average linkage of hierarchical clustering of genes. Pie chart summarizes the results from module differential connectivity (MDC) analysis, where there were more modules lost in *Clock*Δ19 mutant mice than gained. Circos plot depicts 19 WGCNA modules. Enrichment of DE genes for treatments and genotypes is indicated by the semi-circle colors within each module, with increasing warm colors indicating increasing $-\log_{10}(p$ value). The black and brown modules were particularly interesting, as the MDC analysis indicated that these were lost or gained in *Clock*Δ19 mutant mice, respectively, and showed DE enrichment for treatments in *Clock*Δ19 mutant mice. Subsequent analyses focused on the single gained module labeled brown to highlight potential treatment specific pathways and regulators in *Clock*Δ19 mutant mice. The node size indicates the degree of connectivity for any given gene, while light blue indicates DE in VPA, light pink indicates DE in ACY957, and light green indicates DE in both treatments, only in *Clock*Δ19 mutant mice (**C**). To investigate whether there are similar changes between *Clock*Δ19 mutant mice and patients with bipolar disorder, neurons derived from bipolar patients who were nonresponsive to lithium were cultured and treated with the bath application of VPA, ACY957, or vehicle controls for 72 h then collected for RNAseq assays. Meta-analysis of DE transcripts from two patients and two to three clones per patient was used to analyze the top pathways and upstream regulators enriched in VPA- and ACY957-treated human iPSCs ($n = 2$ patients, 2–3 clones per patient, with 2–4 replicates per sample). Top pathways shared between human iPSCs and *Clock*Δ19 mice treated with VPA (**D**) and ACY957 (**E**). Circos plot revealed high degree of overlap between DE transcripts ($p < 0.05$) in human iPSCs and the VTA of *Clock*Δ19 mice (light blue line) for VPA (**D**) and ACY957 (**E**). DE transcripts between human iPSCs and *Clock*Δ19 mice (Venn diagrams). PPI network of significant modules by Metascape for VPA (**D**) and ACY957 (**E**).

on DE transcripts between bipolar patient iPSCs and *Clock*Δ19 mice for VPA and ACY957. We found that several pathways were significantly enriched in both VPA-treated iPSCs and *Clock*Δ19 mice, including transsynaptic signaling, growth factor response, and GPCR ligand binding (Fig. 5D). Several of the DE transcripts shared between human and mouse were related to neurotransmitter (*GAD1* and *GABRD*) and neuropeptide signaling (*NMUR2* and *NPY*) (Fig. 5D). In ACY957-treated iPSCs and *Clock*Δ19 mice, we identified transmembrane receptor protein tyrosine kinase, calcium ion binding, extracellular matrix glycoproteins, and integrin1 pathway among the top pathways shared among humans and mice (Fig. 5E). Several transcripts shared between species being identified as key players in these pathways (e.g., *ADAMTS4, IGFBP5, SGK1, PLP1*, and *CHRNA2*) (Fig. 5E).

To identify potential protein networks of therapeutic action, we used Metascape to construct protein–protein interaction (PPI) networks based on DE transcripts independently for VPA and ACY957 treatments. We found modules involved in GABA synthesis, degradation, and reuptake (SLC32A1, GAD1, and GAD2) that were associated with VPA (Fig. 5D). Interestingly, we also identified a separate PPI module that involves interactions between NPY, ADORA3, OPRD1, DRD3, and NMUR2 (Fig. 5D). These proteins are key regulators of dopamine (DRD3), opioids (OPRD1), adenosine (ADORA3), and circadian-dependent (NMUR2) signaling mechanisms in the midbrain. NMU-dependent signaling (NMU and NMUR2) was also identified in a top PPI module for ACY957 treatment, along with a module largely comprised of zinc finger proteins (Fig. 5E). Together, our findings highlight novel gene and protein signaling pathways involved in the therapeutic response to VPA potentially via HDAC inhibition [44–46].

Discussion

We find that VPA, a commonly prescribed mood stabilizing drug, is able to normalize the manic-like behavioral profile of *Clock*Δ19 mice. This is similar to the effects of chronic lithium treatment, which can also normalize behavioral responses in these mice [17]. Our results with VPA further enhance the predictive validity of the *Clock*Δ19 mice as a model to study the molecular mechanisms of therapeutic action of commonly prescribed medications of bipolar mania, which remain largely unknown. As these therapies have unintended side effects and less than ideal efficacy for many patients with bipolar disorder, understanding the underlying therapeutic mechanisms can lead toward more targeted treatments. One of the many targets of VPA is the ability to inhibit HDAC proteins that are involved in reversing acetylation at histones and other proteins [4, 48].

We decided to implement a pharmacological approach to determine whether HDAC inhibition may underlie the therapeutic effects of VPA using a pan-HDAC inhibitor, SAHA, followed by more targeted inhibitors of specific classes of HDACs. SAHA inhibits both class I and class II HDACs [49], which despite this lack of specificity is still used clinically to treat various cancers and is seemingly well tolerated [50]. Indeed, we find that the broad-spectrum HDAC inhibitor, SAHA has very similar effects on behavior when compared with VPA. More specific HDAC inhibitors are likely to produce more selective effects with the potential for fewer off target effects. To determine more specifically which HDAC proteins may underlie the therapeutic effects of VPA in our assays, we used MS275 and MC1568 compounds. MS275 is a specific inhibitor of class

I HDACs, and MC1568 is a specific inhibitor of class IIa HDACs. We find that only MS275 is able to consistently normalize the behavioral phenotypes of the *Clock*Δ19 mice, suggesting a more important role for class I HDAC proteins in this response. Class I HDAC proteins include HDAC1, HDAC2, HDAC3, and HDAC8 [48]. Therefore, we next examined the efficacy of ACY957, a highly potent and specific inhibitor of HDAC1 and HDAC2 [51]. We find that this drug is also able to normalize behaviors in the *Clock*Δ19 mice, further narrowing down important target proteins. Interestingly, though activity at both HDAC1 and HDAC2 has been previously shown by ACY957 [51], we only find a reduction in *Hdac2* expression after ACY957 treatment in the VTA of *Clock*Δ19 mice.

Notably, we find opposing behavioral results in Wt mice when compared with *Clock*Δ19 mice in some of our pharmacological experiments. This effect was particularly evident with the more selective class I inhibitor ACY957. Previous studies have found that depending on the dose, VPA treatment can lead to anxiolytic- and antidepressive-like behaviors in mice [52]. Furthermore, a study with the class I HDAC inhibitor compound 60 found decreased immobility in the FST in C57BL/6 mice [53]. We and others have previously found that lithium can produce anxiolytic- and antidepressant-like effects in mice that depend on the dose and background strain. However, in *Clock*Δ19 mice, we consistently observe opposite results with a normalization of their inherent manic-like phenotype [17, 19, 54]. This distinction is important in terms of choosing an appropriate animal model for use in understanding the molecular mechanisms that underlie therapeutic effects of these medications. Indeed, lithium and VPA produce very different responses in patients with bipolar disorder versus healthy controls [55–57]. This suggests that these medications have selective effects on altered neuronal processing or activity in individuals with mood disorders which underlies their therapeutic effects.

We chose to use targeted molecular approaches to determine whether HDAC1 or HDAC2 would be sufficient to normalize mania-like behavior. Based on our previous studies [16, 19, 20, 31, 39], we focused on the VTA of *Clock*Δ19 mice where augmented dopamine activity underlies many of the mania-like behaviors in these mice. We created specific shRNA sequences, which were delivered via viral vector into the VTA of *Clock*Δ19 mice. Importantly, only *Hdac2* knockdown led to a normalization of mania-like behavior. To determine whether inhibition of HDAC2 is necessary for the actions of VPA, we employed a virus created to overexpress HDAC2, which was also virally delivered to the VTA. We find that overexpression of HDAC in the VTA blocked the therapeutic actions of VPA in *Clock*Δ19 mice. Taken together, our results show that HDAC2 inhibition in the VTA is both necessary and sufficient to normalize behavior in the *Clock*Δ19 mouse model for bipolar mania. While we focused primarily on the VTA in our studies, future experiments are needed to determine whether HDAC2 inhibition in other brain regions could also be involved in the therapeutic action of VPA, especially since human neuroimaging studies have implicated multiple other neural circuits and brain regions in bipolar disorder [58–60]. Moreover, future studies are also needed to assess whether these compounds also normalize other mania-related phenotypes in the *Clock*Δ19 mice [29], and alter behavior in other mouse models of bipolar disorder [61, 62]. In addition, while we have previously shown that the mood stabilizing compound lithium also reverses the manic-like phenotypes of the *Clock*Δ19 mice [17, 18], and as we show here, VPA, a mood stabilizer, is able to reverse the manic-like phenotypes of the *Clock*Δ19 mice. We do not know if the HDAC inhibitor compounds used in this study would also be effective mood stabilizing agents or might only be effective in treating mania. Previous studies have found that HDAC inhibitors can produce antidepressant effects in animal models of depression. For example, SAHA acts as an antidepressant in a genetic model of depression (Crtc1 KO mice) [63] and MS275 reverses the depressive-like phenotypes of mice following social defeat stress [64], suggesting that they may function as mood stabilizing agents, effecting both depression and mania.

HDAC2 has been implicated in multiple diseases including cardiac hypertrophy [65], Alzheimer's disease [66], Parkinson's disease [67], and a variety of cancers [68]. Neuron-specific overexpression of HDAC2 (but not HDAC1) leads to learning impairments and negatively regulated synaptic plasticity, spine density, and synapse number [69]. Moreover, HDAC2 is upregulated in Alzheimer's disease and inhibition of HDAC2 prevents the cognitive and behavioral impairments in a mouse model of Alzheimer's disease [70]. Interestingly, a recent study found a correlation between the number of microglial-related proteins in the brain and the upregulation of HDAC2 [67]. Since bipolar disorder is also associated with cognitive and behavioral deficits, along with increased inflammatory responses including microglial activation [71], it is possible that HDAC2 plays a role in these phenotypes and that inhibition is therapeutic. Moreover, a conditional knockout of HDAC2 in glutamatergic pyramidal neurons leads to a protective effect against psychedelic drugs known to induce psychotic like phenotypes, suggesting that HDAC2 inhibition may also be beneficial in the treatment of psychosis [72].

HDAC inhibition is known to influence transcription of a number of genes. In general, hyperacetylation of histones is associated with relaxed chromatin state leading to increased gene transcription. We find that class I HDAC inhibition by

ACY957 in *Clock*Δ19 mice lead to the differential expression of 24 transcripts shared with VPA. Several of these transcripts are also found in the only module (i.e., brown) identified by WGCNA and MDC analyses to be highly coordinated in the VTA of *Clock*Δ19 mice in response to VPA and ACY957. For example, *Fbxo32, Bcas1*, and *Kcnk13* are altered by both VPA and ACY957 and also are hub genes in the brown module. Interestingly, FBXO32 interacts with endophilin-A proteins, which are highly expressed in presynaptic dopamine terminals and modulate the release of dopamine into the striatum [73]. Regulation of endophilin-A proteins and others via the inhibition of the ubiquitin-proteasome system leads to the depletion of striatal dopamine [73]. Given that *Fbxo3* was downregulated by both ACY957 and VPA and elevated dopamine neurotransmission is a hallmark of *Clock*Δ19 mice [16, 20, 31], destabilization of the ubiquitin-proteasome system via an HDAC2-dependent mechanism may lead to a reduction in dopamine cell firing and release and mania-like behaviors in these mice. In addition, the other hub genes, *Bcas1* and *Kcnk13*, have also been shown to be involved in the regulation of dopamine neurotransmission and related behaviors [74, 75]. KCNK13 is a leaky potassium channel that is highly expressed in the VTA that modulates dopamine cell firing [76]. Although speculative, downregulation of this channel may be a novel target that mediates the therapeutic actions of VPA via HDAC inhibition and could be involved in both the pathology and treatment of bipolar disorder [77].

We measured transcriptional changes in human iPSCs derived from bipolar patients that were nonresponsive to lithium. Interestingly, both VPA and ACY957 treatment produced similar changes in transcript expression including genes involved in transsynaptic signaling, neurotransmission, and ion transport. There are also similarities between changes found in iPSCs and *Clock*Δ19 mice, such as transsynaptic signaling, growth factor response, and GPCR ligand binding, which includes many genes involved in cellular growth and plasticity. Additionally, the majority of the pathways enriched between ACY957-treated human iPSCs and *Clock*Δ19 mice are related to the extracellular matrix and synaptic morphology (e.g., extracellular matrix glycoproteins and glycosaminoglycan binding). The extracellular matrix is critical for both synaptic formation and degradation [78]. Studies have found that HDAC2 negatively regulates memory formation and synaptic plasticity, and some of these actions are through interaction with the transcription factors Sp1 and Sp3 [69, 79, 80]. We identified SP1 as a top upstream regulator in human iPSCs targeted by both VPA and ACY957. Thus, treatments like VPA that inhibit HDAC2 may promote synaptic plasticity via dynamic regulation of proteins involved in extracellular matrix formation and growth response factors [81].

We conducted both upstream regulator predictions and PPI network analyses in an effort to reveal primary mediators of therapeutic action of VPA via HDAC inhibition. Both of these approaches highlighted the potential for circadian-dependent regulation of molecular signaling in the VTA and human iPSCs from patients with bipolar disorder in the therapeutic response to VPA and ACY957. Notably, we found both ARNTL (BMAL1) and CLOCK among the top upstream regulators predicted to be involved in the transcriptional response to ACY957. NFKB1 and RELA are also top upstream regulators. Both HDAC2 and ARNTL are known to modulate the NF-κB-dependent gene expression in multiple ways [82–84]. Furthermore, we identified NMU-dependent signaling (i.e., NMU and NMUR2) to be consistently related to the transcriptional response in humans and mice across both VPA and ACY957 treatments. NMU is widely expressed in peripheral tissues and the brain and acts via two GPCRs, including NMUR2 [85]. NMUR2 is predominantly expressed in the brain and has previously been shown to attenuate striatal dopamine release when overexpressed [86]. Intriguingly, NMU has also been shown to be essential to circadian regulation in other regions of the rodent brain [87, 88]. Future studies will investigate whether NMU-dependent signaling is involved in the therapeutic response to VPA and other HDAC inhibitors in the VTA. These studies may be especially important as circadian rhythms may be involved in both the pathophysiology of bipolar disorder and its treatment [89, 90].

In conclusion, we demonstrate that compounds that inhibit HDAC2, as well as HDAC2 inhibition in the VTA, result in the normalization of manic-like behavior in the *Clock*Δ19 model of bipolar mania. We also find that overexpression of HDAC2 in the VTA is sufficient to block the normally therapeutic actions of VPA. Future studies will investigate the molecular and cellular mechanisms by which HDAC2 inhibition leads to these behavioral changes, and further examine the pathways underlying potential sex-specific effects of HDAC inhibition and VPA on mania-like behaviors in female mice. Better understanding of these mechanisms along with our current studies begins to pave the way for more targeted treatments for bipolar disorder.

Methods

Mice

Homozygous *Clock*Δ19 and Wt littermates (originally provided by Dr. Joe Takahashi) [24] were bred from heterozygotes and maintained on a BALB/c background. This point mutation results in a dominant-negative protein that

still binds DNA and interacts with partner, BMAL1, yet fails to activate transcription [91]. Adult mice were group housed and maintained on a12:12 light–dark cycle with lights on (Zeitgeber Time (ZT0)) at 0700 and off at 1900 (ZT12). Mice were provided ad libitum food and water unless otherwise indicated. All procedures were approved by the University of Pittsburgh IACUC.

Pharmacological treatments

Adult male and female Wt or *Clock*Δ19 mice (12–18 weeks) were treated with a variety of HDAC inhibitors, which increase acetylation of histones H3 and H4 (Supplementary Fig. 1). Sodium VPA (VPA; Sigma-Aldrich) was compounded in custom chow (Teklad Animal Diets, Harlan Laboratories) at 20 g/kg, previously demonstrated in rodents to achieve blood levels within the therapeutic window for humans [36, 92, 93]. The broad-spectrum inhibitor SAHA acid (LC Laboratories), which inhibits class I and class II HDACs, was complexed with 2-hydroxypropyl-β-cyclodextrin (HOP-β-CD) and delivered through the drinking water at a target dose of 100 mg/kg. As previously shown, SAHA complexed with HOP-β-CD improves solubility and readily crosses the blood brain barrier [94]. For both VPA and SAHA experiments, mice underwent a 1-week habituation period to the vehicle chow or drinking solution. Separate cohorts of mice were either treated with MS275 (Selleck Chemicals), a class I-specific HDAC inhibitor (20 mg/kg, 10 ml/kg i.p. injection, 1% w/v of DMSO with 0.5% w/v carboxymethylcellulose), or MC1568 (Selleck Chemicals), a class IIa-specific inhibitor (20 mg/kg, 10 ml/kg i.p. injection, 1% w/v of DMSO with 0.5% w/v carboxymethylcellulose). ACY957 (Regenacy Pharmaceuticals Inc.) was also used as an HDAC1/2 inhibitor (10 mg/kg, 10 ml/kg i.p. injection, 0.5% w/v hydroxypropyl methylcellulose (Sigma-Aldrich) in MilliQ water). Control cohorts of mice received the respective vehicle for each treatment, which included either 1% w/v DMSO and 0.5% w/v carboxymethylcellulose, or 0.5% w/v hydroxypropyl methylcellulose in MilliQ water. Mice were administered compounds daily for 14 days including daily during behavioral testing. Injections immediately followed the behavioral tests.

Analysis of plasma and brain concentrations

Mice were administered ACY957 (10 mg/kg, 10 ml/kg i.p. injection, hydroxypropyl methylcellulose) then sacrificed either 1, 4, 8, or 24 h after to collect blood plasma and brain. Samples were sent to Regenacy Pharmaceuticals, Inc. to measure tissue concentrations of ACY957 via HPLC (Shanghai Chempartner Co., Ltd.) based on standard curves of known concentrations.

Behavioral testing

These behavioral assays were performed between ZT4 and ZT8 in the following order on successive days: locomotor activity, open field, dark/light box, EPM, and FST. Male and female Wt and *Clock*Δ19 mice treated with VEH, VPA, SAHA, MS275, MC1568, or ACY957 were habituated to testing rooms for 1 h prior to testing. Chambers were cleaned with 70% ethanol and allowed to dry between animals. Mice were placed into a novel environment inside automated locomotor activity chambers equipped with infrared photobeams measuring horizontal activity (Kinderscientific Smart Cage Rack System; 9.5″ × 18″). Activity measurements began immediately and were continuously collected in 5-min bins. Locomotor activity was measured as number of beam breaks over a 1-h test. Mice were placed in the center of a novel open field environment (61 cm^3 plexiglass arena) with a clear floor and solid black walls. Mice were allowed to explore the arena for 10 min, and time spent, distance traveled, and entries into the center (20 cm^2 area) of the arena were recorded. For the dark/light box (KinderScientific Smart Cage Rack System), mice were place into the dark side (~100 lux) of the box with a small doorway that allowed free exploration of both dark and light sides of the box for 10 min. Latency to enter the light side and time spent on the light side of the apparatus were measured. Mice were placed in the center of an EPM in dim light (~20 lux). The EPM consisted of two plastic open arms perpendicular to two closed arms (30 × 5 cm) and was elevated above the ground (60 cm). Behavior was recorded for 5 min and video tracking software was used to quantify the time spent in the closed and open arms, as well as number of entries into the arms (Ethovision; Noldus, Leesburg, VA, USA). Manual scoring of EPM was also conducted for verification. For FST, mice were placed into a 6 L pyrex glass beaker containing 3 L of water (24 ± 1 °C) for 6 min. Each session was recorded and 2–6 min was scored manually by trained, blind experimenters. Latency to immobility was determined as the first cessation of all movement, while total immobility was measured as the time spent without any motion except for single limb paddling to maintain flotation.

Construction and validation of shRNA and overexpression constructs

A short hairpin RNA (shRNA) against HDAC1 and HDAC2 was constructed by selecting a unique 24 base sequence in the coding region of *Hdac1* or *Hdac2* mRNA (Supplementary Table 3). These shRNAs were tested for specificity and do not impact expression of other class 1 *Hdacs* (Supplementary Fig. 3). For the scrambled shRNA, a random sequence of 24 bases was used with no sequence

similarities to any known genes. An antisense sequence of the selected mRNA region followed by a miR23 loop of ten nucleotides (CTTCCTGTCA) was added at the 5′end of the sequence. The first and last bases of the forward and reverse sequences were modified to G or A, respectively, to promote strand bias. These shRNAs were designed as synthetic duplexes with overhang ends identical to those created by SapI and XbaI restriction enzyme digestion. The annealed oligonucleotides were cloned into the adeno-associated virus (AAV2) plasmid expressing green fluorescent protein (Stratagene, La Jolla, CA). Plasmid constructs were validated for specificity of knockdown of *Hdac1* or *Hdac2* using transfection of PC12 cells followed by GFP-based cell sorting and gene expression assays. Viral production was completed by University of North Carolina Vector Core. As previously described, overexpression of HDAC2 was achieved by a HDAC2 cDNA containing herpes simplex virus (HSV) [95, 96].

Viral manipulations

Male Wt and *Clock*Δ19 mice were anesthetized with isoflurane to undergo stereotaxic brain surgery to bilaterally inject scrambled or shRNA containing AAVs (1 µl/side) into the VTA (relative to bregma: 7°, AP −3.2, ML ±1.0, DV −4.6) [39]. Mice recovered for 2–3 weeks in their home cages prior to behavioral testing. In a separate cohort, male *Clock*Δ19 mice were bilaterally injected with HSV-HDAC2 to achieve overexpression in the VTA (1 µl/side). Mice then recovered for 3 days prior to behavioral testing. For 1 week prior to and following surgery, these mice consumed either control or VPA-compounded chow. After behavioral testing, immunohistochemistry was performed to determine the extent of viral transduction. Mice were excluded if viral spread was not localized to the VTA, with viral spread through the injection tract, or with asymmetrical infection between hemispheres (~10% of mice).

Immunohistochemistry

Mice were deeply anesthetized with ketamine (100 mg/kg) and xylazine (10 mg/kg) then perfused with 4% paraformaldehyde in phosphate-buffered saline (PBS, pH 7.4). Brains were postfixed in 4% paraformaldehyde for 24 h, then transferred to 30% sucrose solution. Sections (30 µm) were processed for GFP, TH, and DAPI. Floating sections were rinsed with 1X PBS then blocked with PBS and 3% Donkey Serum (0.3% Triton-X/PBS) for 1 h to incubate overnight at room temperature with TH antibody (1:5000, mouse, Sigma-Aldrich) and GFP antibody (1:20,000, rabbit, Abcam, Cambridge, MA, USA). Sections were rinsed with 1X PBS, incubated in secondary fluorophore antibodies (1:400, donkey anti-rabbit 488 or donkey anti-mouse 546) for 2 h at room temperature on rotary shaker. Sections were washed with 1X PBS, mounted and cover slipped with DAPI mounting medium (Vectashield, Burlingame, CA, USA). Sections were imaged with an epifluorescent microscope (×4, ×10, and ×40).

RNA isolation, cDNA, and qPCR

Mice were sacrificed using rapid cervical dislocation and brains were rapidly extracted, frozen, and stored at −80 °C for further processing. Microdissected VTA punches (viral GFP + punches were visualized using NightSea BlueStar flashlight, Lexington, MA, USA) were homogenized mechanically using a QIAshredder spin column (Qiagen, Germantown, MD, USA). Total RNA was extracted using RNeasy Plus Micro Kits (Qiagen) following the manufacturer's protocol. gDNA was eliminated prior to extraction with the provided gDNA Eliminator column. Concentration and quality of total RNA were determined via NanoDrop 2000 UV–Vis spectrophotometer (Thermo Fisher Scientific, Waltham, MA, USA). cDNA was synthesized from 100 ng of total RNA with SuperScript VILO Master Mix (Invitrogen, Carlsbad, CA, USA). cDNA was used to measure gene expression with qPCR. Briefly, sample cDNA (1 ng) was loaded with Power SYBR Green PCR Master Mix (Thermo Fisher Scientific), forward and reverse primers for specific genes of interest. Primers were tested for efficiency, specificity, and absence of primer dimers. Duplicate samples were amplified on a 96-well plate with the Applied Biosystems 7900HT Fast Real-Time PCR System (Applied Biosystems, Foster City, CA, USA). Relative gene expression was calculated using the $2^{-\Delta\Delta Ct}$ method, normalized to reference gene *Gapdh*, and reported as mean ± SEM. A list of primers used in this study is given in Supplementary Table 3.

Human iPSC cultures

Human fibroblasts or lymphoblasts from multiple patients were reprogrammed to hiPSCs via non-integrating episomal-mediated, lentivirus-mediated, or retrovirus mediated gene transfer, characterized, and differentiated to NPCs, as previously described [46, 97–100]. We used iPSCs from two patients diagnosed with bipolar disorder and classified as Lithium NonResponsive (Pt-LiNR-1 and Pt-LiNR-2). Patient selection criteria, clinical evaluation and classification were conducted as thoroughly described previously [46, 101]. We use two separate clones from each patient in these experiments. Differentiation into neurons was similar to techniques described previously [46]. Neurons were cultured for 4 weeks prior to pharmacological experiments. Neurons were cultured in four 12-well plates of cells with two plates as technical replicates for each patient. Each of

the wells of the 12-well plate were treated with either vehicle (water), VPA (1 mM), or ACY957 (3 μM), repeated in quadruplicates (2 patients × 2 clones × 3 treatments × 4 replicates = 48 samples). Cells were treated for 72 h with daily media and compound changes, then collected, washed (1X PBS), and pelleted then flash frozen for RNA extraction.

RNA sequencing

Brains were extracted and flash frozen from adult male *Clock*Δ19 or Wt mice treated with VPA, ACY957, or their respective vehicles for 14 days (see above). Tissue was collected at ZT6, ~24 h after the last treatment. Multiple bilateral 1 mm punches were taken centered over the VTA. Individual mice were used as biological replicates (8 mice × 2 genotypes × 4 treatments = 64 samples). Human iPSCs and mouse brain tissue punches were homogenized and total RNA was isolated using the RNeasy Plus Micro Kit (Qiagen, Hilden, Germany). RNA quantity and quality were assessed using fluorometry (Qubit RNA Broad Range Assay Kit and Fluorometer; Invitrogen, Carlsbad, CA) and chromatography (Bioanalyzer and RNA 6000 Nano Kit; Agilent, Santa Clara, CA), respectively. Libraries were prepared using TruSeq Stranded mRNA (PolyA+) kit (Illumina, San Diego, CA) and sequenced by Illumina NextSeq 500. The read length was 75 bp with 30–40 M reads per sample. FastQC (v0.11.3) was performed to assess data quality. TopHat2 (v2.0.9) aligned the reads to the mouse reference genome (*Mus musculus* UCSC mm10) and to the Ensembl human reference genome (GRCh38.p13) using default parameters [102]. Alignments were then converted to expression count data using HTseq (v0.6.1) with default union mode [103]. The RNAseq count data were transformed to log2 count data using voom function of the Bioconductor limma package [104, 105]. Data have been deposited into GEO, accession numbers GSE160761 and GSE160374.

Analysis of histone acetylation

Histones were isolated for western immunoblotting as in Fischer et al. [106]. Brain tissue was homogenized in TX buffer (50 mM Tris HCl, 150 mM NaCl, 2 mM EDTA, 1% Triton-100) and incubated on ice for 15 min. The samples were centrifuged at 2000 RPM at 4 °C for 10 min. The samples were washed in TX buffer. The pellet was then dissolved in TX buffer containing 0.2 M HCl and incubated on ice for 30 min followed by centrifugation at 10,000 RPM at 4 °C for 10 min. The supernatant was isolated and used directly for immunoblotting. Aliquots of sample were combined 1:1 in Laemmli SDS sample buffer (Bio-World, Dublin, OH), and heated at 95 °C for 5 min. Samples were loaded and electrophoresed on a precast 12% Tris-glycine extended gel (Biorad, Hercules, CA) at 120 V for ~90 min in 1XTGS buffer (Biorad, Hercules, CA). Proteins were transferred at 90 V at 4 °C for 45 min onto Immunobilon-FL transfer membrane (Millipore). Membranes were blocked (Odyssey Blocking Buffer; LI-COR Biosciences, Lincoln, NE, USA) and incubated with primary antibodies at 4 °C overnight. The following primary antibodies were used: acetylated histone H3 (1:1000; Millipore #06-599), acetylated histone H4 (1:1000; Millipore #06-866), total histone H3 (1:1000; Millipore #07-690), total histone H4 (1:1000; Millipore #04-858). Blots were stripped following application of the acetylated histone and reprobed with total histone antibodies (NewBlot Stripping Buffer, LI-COR). Optical densities were quantified by NIH ImageJ software and normalized to the reference protein. These values were then expressed as a ratio of acetylated histones to total histones.

Statistical analyses

Differential expression

Transcripts were eliminated based on zero counts then filtered by the lowest 25% across all samples. Differential expression analysis was conducted by limma-voom comparing Wt to *Clock*Δ19 mice treated with VEH, VPA, or ACY957. For human iPSCs, differential expression analysis was conducted by limma-voom comparing VPA or ACY957 to VEH within patient for each clone and replicate. Differentially expressed (DE) genes were selected based on fold change (FC) ≤ -1.2 or ≥ 1.2 and $p \leq 0.05$. Venn diagrams were used to compare the overlap of DE genes between groups. Heat maps were constructed using logFC of gene expression.

Pathway enrichment and upstream regulator predictions

Overrepresentation of pathway and gene ontology (GO) categories was assessed using Metascape (http://www.metascape.org), with expressed genes as background. We assessed enrichment using GO, KEGG, Hallmark, Canonical Pathways, Reactome, BioCarta, and CORUM (only expressed genes were used as the background data set; pathways with <20 genes were excluded). Upstream regulators were restricted to transcription factors. Pathway enrichment was performed for each brain region separately and for the list of DE genes that were shared across brain regions.

Weighted gene co-expression network analysis (WGCNA)

WGCNA was used to identify gene modules with similar expression patterns across samples, built on samples from

*Clock*Δ19 mice [107, 108]. Module preservation analysis was performed to determine whether the modules identified were robust [43]. Analysis was based on the module size and compared to a network built on a subset of *Clock*Δ19 mice, where higher *Z*-scores represent robust evidence that the observed value of the preservation statistic is significantly higher than expected by chance. Only modules with scores >10 are considered highly preserved and used in downstream analyses. The MCD metric was used to quantify co-expression differences between Wt and *Clock*Δ19 by calculating a ratio of the connectivity of gene pairs in a module from Wt mice to those from *Clock*Δ19 mice. MDC > 1 indicates gain of connectivity, while MDC < 1 indicates loss of connectivity. To statistically test the significance of MDC, we estimated the *p* value based on two types of shuffling schemes: (1) shuffled samples—adjacent matrix with nonrandom nodes but random connections; (2) shuffled genes—adjacent matrix with random nodes but nonrandom connections. Data were permuted 1000 times. *p* values were converted to *q* values following Benjamini Hochberg procedure, and MDC $q < 0.05$ was considered significant. Enrichment of DE genes was examined within each module by genotype and treatments. ARACNe was used to identify hub and stress-specific hub genes for network analysis. Briefly, a gene is considered a hub if the N-hob neighborhood nodes (NHNN) for that gene is significantly higher than the average NHNN. Cytoscape (v3.8.0) was used to generate networks, with correlations > 0.98 plotted in the networks.

Other analyses

Two-way ANOVA was used to examine main effects of genotype and interactions for molecular, physiological, and behavioral experiments. Significant interactions (genotype × treatment) were followed by post hoc tests (Tukey's or Sidak's, where appropriate). Data are expressed as mean ± SEM with a two-tailed $\alpha = 0.05$ considered statistically significant. Data were processed using Microsoft Excel, ImageJ, and GraphPad Prism software.

Acknowledgements We thank Heather Buresch, Mark Brown, and Emily W. Sedlock for mouse husbandry, coordination, and genotyping. The studies were supported by an IMHRO Rising Star Award, the Brain and Behavior Research Foundation (NARSAD Independent Investigator Award), MH106460, MH115241, MH111601 to CAM; Brain and Behavior Research Foundation (NARSAD Young Investigator Award), K01DA038654 to RWL.

Author contributions CAM, RWL, KDK, and LMD wrote the paper. CAM, RWL, EYS, GCT, and MBJ designed experiments. RLW, ARO, RNA, AW, AC, BTDT, DB-K, MBJ, PKP, XZ, EF, HZ, JO-S, MAH, LMD, and KDK performed experiments. RWL, XX, WZ, ZH, and XZ analyzed data.

Compliance with ethical standards

Conflict of interest MBJ is a full type employee of Regenacy Pharmaceuticals. Studies involving the ACY compound were funded through a contract with Regenacy Pharmaceuticals Inc. to RWL. All other authors declare no conflict of interest.

Publisher's note Springer Nature remains neutral with regard to jurisdictional claims in published maps and institutional affiliations.

References

1. Lopez-Munoz F, Shen WW, D'Ocon P, Romero A, Alamo C. A history of the pharmacological treatment of bipolar disorder. Int J Mol Sci. 2018;19:2143.
2. Macdonald RL, Kelly KM. Antiepileptic drug mechanisms of action. Epilepsia. 1995;36:S2–12.
3. Gould TD, Quiroz JA, Singh J, Zarate CA, Manji HK. Emerging experimental therapeutics for bipolar disorder: insights from the molecular and cellular actions of current mood stabilizers. Mol Psychiatry. 2004;9:734–55.
4. Phiel CJ, Zhang F, Huang EY, Guenther MG, Lazar MA, Klein PS. Histone deacetylase is a direct target of valproic acid, a potent anticonvulsant, mood stabilizer, and teratogen. J Biol Chem. 2001;276:36734–41.
5. Chiu CT, Wang Z, Hunsberger JG, Chuang DM. Therapeutic potential of mood stabilizers lithium and valproic acid: beyond bipolar disorder. Pharmacol Rev. 2013;65:105–42.
6. Nestler EJ, Pena CJ, Kundakovic M, Mitchell A, Akbarian S. Epigenetic basis of mental illness. Neuroscientist. 2016;22:447–63.
7. Morris MJ, Monteggia LM. Unique functional roles for class I and class II histone deacetylases in central nervous system development and function. Int J Dev Neurosci. 2013;31:370–81.
8. Dai Y, Faller DV. Transcription regulation by class III histone deacetylases (HDACs)-sirtuins. Transl Oncogenomics. 2008;3:53–65.
9. Baltan S, Bachleda A, Morrison RS, Murphy SP. Expression of histone deacetylases in cellular compartments of the mouse brain and the effects of ischemia. Transl Stroke Res. 2011;2:411–23.
10. Ryu H, Lee J, Olofsson BA, Mwidau A, Dedeoglu A, Escudero M, et al. Histone deacetylase inhibitors prevent oxidative neuronal death independent of expanded polyglutamine repeats via an Sp1-dependent pathway. Proc Natl Acad Sci USA. 2003;100:4281–6.
11. Machado-Vieira R, Ibrahim L, Zarate CA Jr. Histone deacetylases and mood disorders: epigenetic programming in gene-environment interactions. CNS Neurosci Ther. 2011;17:699–704.
12. Benes FM, Lim B, Matzilevich D, Walsh JP, Subburaju S, Minns M. Regulation of the GABA cell phenotype in hippocampus of schizophrenics and bipolars. Proc Natl Acad Sci USA. 2007;104:10164–9.
13. Tseng CJ, Gilbert TM, Catanese MC, Hightower BG, Peters AT, Parmar AJ, et al. In vivo human brain expression of histone deacetylases in bipolar disorder. Transl Psychiatry. 2020;10:224.
14. Arent CO, Valvassori SS, Fries GR, Stertz L, Ferreira CL, Lopes-Borges J, et al. Neuroanatomical profile of antimaniac effects of histone deacetylases inhibitors. Mol Neurobiol. 2011;43:207–14.
15. Varela RB, Resende WR, Dal-Pont GC, Gava FF, Tye SJ, Quevedo J, et al. HDAC inhibitors reverse mania-like behavior and modulate epigenetic regulatory enzymes in an animal model of mania induced by Ouabain. Pharmacol Biochem Behav. 2020;193:172917.
16. McClung CA, Sidiropoulou K, Vitaterna M, Takahashi JS, White FJ, Cooper DC, et al. Regulation of dopaminergic

transmission and cocaine reward by the Clock gene. Proc Natl Acad Sci USA. 2005;102:9377–81.
17. Roybal K, Theobold D, Graham A, DiNieri JA, Russo SJ, Krishnan V, et al. Mania-like behavior induced by disruption of CLOCK. Proc Natl Acad Sci USA. 2007;104:6406–11.
18. Arey R, McClung CA. An inhibitor of casein kinase 1 epsilon/delta partially normalizes the manic-like behaviors of the ClockDelta19 mouse. Behav= Pharmacol. 2012;23:392–6.
19. Arey RN, Enwright JF 3rd, Spencer SM, Falcon E, Ozburn AR, Ghose S, et al. An important role for cholecystokinin, a CLOCK target gene, in the development and treatment of manic-like behaviors. Mol Psychiatry. 2014;19:342–50.
20. Sidor MM, Spencer SM, Dzirasa K, Parekh PK, Tye KM, Warden MR, et al. Daytime spikes in dopaminergic activity drive rapid mood-cycling in mice. Mol Psychiatry. 2015;20:1406–19.
21. Logan RW, McClung CA. Animal models of bipolar mania: the past, present and future. Neuroscience. 2016;321:163–88.
22. Parekh PK, Sidor MM, Gillman A, Becker-Krail D, Bettelini L, Arban R, et al. Antimanic efficacy of a novel Kv3 potassium channel modulator. Neuropsychopharmacology. 2018;43:435–44.
23. King DP, Takahashi JS. Molecular genetics of circadian rhythms in mammals. Annu Rev Neurosci. 2000;23:713–42.
24. King DP, Zhao Y, Sangoram AM, Wilsbacher LD, Tanaka M, Antoch MP, et al. Positional cloning of the mouse circadian clock gene. Cell. 1997;89:641–53.
25. Naylor E, Bergmann BM, Krauski K, Zee PC, Takahashi JS, Vitaterna MH, et al. The circadian clock mutation alters sleep homeostasis in the mouse. J Neurosci. 2000;20:8138–43.
26. Easton A, Arbuzova J, Turek FW. The circadian Clock mutation increases exploratory activity and escape-seeking behavior. Genes Brain Behav. 2003;2:11–19.
27. Ozburn AR, Falcon E, Mukherjee S, Gillman A, Arey R, Spencer S, et al. The role of clock in ethanol-related behaviors. Neuropsychopharmacology. 2013;38:2393–2400.
28. Ozburn AR, Larson EB, Self DW, McClung CA. Cocaine self-administration behaviors in ClockDelta19 mice. Psychopharmacology. 2012;223:169–77.
29. van Enkhuizen J, Minassian A, Young JW. Further evidence for ClockDelta19 mice as a model for bipolar disorder mania using cross-species tests of exploration and sensorimotor gating. Behav Brain Res. 2013;249:44–54.
30. McClung CA, Nestler EJ, Zachariou V. Regulation of gene expression by chronic morphine and morphine withdrawal in the locus ceruleus and ventral tegmental area. J Neurosci. 2005;25:6005–15.
31. Coque L, Mukherjee S, Cao JL, Spencer S, Marvin M, Falcon E, et al. Specific role of VTA dopamine neuronal firing rates and morphology in the reversal of anxiety-related, but not depression-related behavior in the ClockDelta19 mouse model of mania. Neuropsychopharmacology. 2011;36:1478–88.
32. Mukherjee S, Coque L, Cao JL, Kumar J, Chakravarty S, Asaithamby A, et al. Knockdown of Clock in the ventral tegmental area through RNA interference results in a mixed state of mania and depression-like behavior. Biol Psychiatry. 2010;68:503–11.
33. Berk M, Dodd S, Kauer-Sant'anna M, Malhi GS, Bourin M, Kapczinski F, et al. Dopamine dysregulation syndrome: implications for a dopamine hypothesis of bipolar disorder. Acta Psychiatr Scand Supplementu. 2007;434:41–9.
34. Ashok AH, Marques TR, Jauhar S, Nour MM, Goodwin GM, Young AH, et al. The dopamine hypothesis of bipolar affective disorder: the state of the art and implications for treatment. Mol Psychiatry. 2017;22:666–79.
35. Abler B, Greenhouse I, Ongur D, Walter H, Heckers S. Abnormal reward system activation in mania. Neuropsychopharmacology. 2008;33:2217–27.
36. van Enkhuizen J, Geyer MA, Kooistra K, Young JW. Chronic valproate attenuates some, but not all, facets of mania-like behaviour in mice. Int J Neuropsychopharmacol. 2013;16:1021–31.
37. Simonini MV, Camargo LM, Dong E, Maloku E, Veldic M, Costa E, et al. The benzamide MS-275 is a potent, long-lasting brain region-selective inhibitor of histone deacetylases. Proc Natl Acad Sci USA. 2006;103:1587–92.
38. Kassis H, Shehadah A, Li C, Zhang Y, Cui Y, Roberts C, et al. Class IIa histone deacetylases affect neuronal remodeling and functional outcome after stroke. Neurochem Int. 2016;96:24–31.
39. Logan RW, Parekh PK, Kaplan GN, Becker-Krail DD, Williams WP 3rd, Yamaguchi S, et al. NAD+ cellular redox and SIRT1 regulate the diurnal rhythms of tyrosine hydroxylase and conditioned cocaine reward. Mol Psychiatry 2018;24:1668–84.
40. Ang SL. Transcriptional control of midbrain dopaminergic neuron development. Development. 2006;133:3499–506.
41. Lydall GJ, Bass NJ, McQuillin A, Lawrence J, Anjorin A, Kandaswamy R, et al. Confirmation of prior evidence of genetic susceptibility to alcoholism in a genome-wide association study of comorbid alcoholism and bipolar disorder. Psychiatr Genet. 2011;21:294–306.
42. McCarthy MJ, Nievergelt CM, Kelsoe JR, Welsh DK. A survey of genomic studies supports association of circadian clock genes with bipolar disorder spectrum illnesses and lithium response. PLoS ONE. 2012;7:e32091.
43. Langfelder P, Luo R, Oldham MC, Horvath S. Is my network module preserved and reproducible? PLoS Comput Biol. 2011;7:e1001057.
44. Stern S, Santos R, Marchetto MC, Mendes APD, Rouleau GA, Biesmans S, et al. Neurons derived from patients with bipolar disorder divide into intrinsically different sub-populations of neurons, predicting the patients' responsiveness to lithium. Mol Psychiatry. 2018;23:1453–65.
45. Mertens J, Wang QW, Kim Y, Yu DX, Pham S, Yang B, et al. Differential responses to lithium in hyperexcitable neurons from patients with bipolar disorder. Nature. 2015;527:95–9.
46. Tobe BTD, Crain AM, Winquist AM, Calabrese B, Makihara H, Zhao WN, et al. Probing the lithium-response pathway in hiPSCs implicates the phosphoregulatory set-point for a cytoskeletal modulator in bipolar pathogenesis. Proc Natl Acad Sci USA. 2017;114:E4462–71.
47. Zhou Y, Zhou B, Pache L, Chang M, Khodabakhshi AH, Tanaseichuk O, et al. Metascape provides a biologist-oriented resource for the analysis of systems-level datasets. Nat Commun. 2019;10:1523.
48. Delcuve GP, Khan DH, Davie JR. Roles of histone deacetylases in epigenetic regulation: emerging paradigms from studies with inhibitors. Clin Epigenetics. 2012;4:5.
49. Marks PA, Dokmanovic M. Histone deacetylase inhibitors: discovery and development as anticancer agents. Expert Opin Investig Drugs. 2005;14:1497–511.
50. Bubna AK. Vorinostat—an overview. Indian J Dermatol. 2015;60:419.
51. Shearstone JR, Golonzhka O, Chonkar A, Tamang D, van Duzer JH, Jones SS, et al. Chemical inhibition of histone deacetylases 1 and 2 induces fetal hemoglobin through activation of GATA2. PloS ONE. 2016;11:e0153767.
52. Lima IVA, Almeida-Santos AF, Ferreira-Vieira TH, Aguiar DC, Ribeiro FM, Campos AC, et al. Antidepressant-like effect of valproic acid-Possible involvement of PI3K/Akt/mTOR pathway. Behav Brain Res. 2017;329:166–71.
53. Schroeder FA, Lewis MC, Fass DM, Wagner FF, Zhang YL, Hennig KM, et al. A selective HDAC 1/2 inhibitor modulates chromatin and gene expression in brain and alters mouse behavior in two mood-related tests. PLoS ONE. 2013;8:e71323.

54. Can A, Blackwell RA, Piantadosi SC, Dao DT, O'Donnell KC, Gould TD. Antidepressant-like responses to lithium in genetically diverse mouse strains. Genes Brain Behav. 2011;10:434–43.
55. White K, Bohart R, Whipple K, Boyd J. Lithium effects on normal subjects. Relationships to plasma and RBC lithium levels. Int Pharmacopsychiatry. 1979;14:176–83.
56. Aldenkamp AP, Arends J, Bootsma HP, Diepman L, Hulsman J, Lambrechts D, et al. Randomized double-blind parallel-group study comparing cognitive effects of a low-dose lamotrigine with valproate and placebo in healthy volunteers. Epilepsia. 2002;43:19–26.
57. Cipriani A, Reid K, Young AH, Macritchie K, Geddes J. Valproic acid, valproate and divalproex in the maintenance treatment of bipolar disorder. Cochrane Database Syst Rev. 2013:CD003196.
58. Hallahan B, Newell J, Soares JC, Brambilla P, Strakowski SM, Fleck DE, et al. Structural magnetic resonance imaging in bipolar disorder: an international collaborative mega-analysis of individual adult patient data. Biol Psychiatry. 2011;69:326–35.
59. Hibar DP, Westlye LT, Doan NT, Jahanshad N, Cheung JW, Ching CRK, et al. Cortical abnormalities in bipolar disorder: an MRI analysis of 6503 individuals from the ENIGMA Bipolar Disorder Working Group. Mol Psychiatry. 2018;23:932–42.
60. Strakowski SM, Eliassen JC, Lamy M, Cerullo MA, Allendorfer JB, Madore M, et al. Functional magnetic resonance imaging brain activation in bipolar mania: evidence for disruption of the ventrolateral prefrontal-amygdala emotional pathway. Biol Psychiatry. 2011;69:381–8.
61. Milienne-Petiot M, Kesby JP, Graves M, van Enkhuizen J, Semenova S, Minassian A, et al. The effects of reduced dopamine transporter function and chronic lithium on motivation, probabilistic learning, and neurochemistry in mice: modeling bipolar mania. Neuropharmacology. 2017;113:260–70.
62. Young JW, Cope ZA, Romoli B, Schrurs E, Aniek J, van Enkhuizen J, et al. Mice with reduced DAT levels recreate seasonal-induced switching between states in bipolar disorder. Neuropsychopharmacology. 2018;43:1721–31.
63. Meylan EM, Halfon O, Magistretti PJ, Cardinaux JR. The HDAC inhibitor SAHA improves depressive-like behavior of CRTC1-deficient mice: possible relevance for treatment-resistant depression. Neuropharmacology. 2016;107:111–21.
64. Covington HE 3rd, Maze I, Vialou V, Nestler EJ. Antidepressant action of HDAC inhibition in the prefrontal cortex. Neuroscience. 2015;298:329–35.
65. Eom GH, Nam YS, Oh JG, Choe N, Min HK, Yoo EK, et al. Regulation of acetylation of histone deacetylase 2 by p300/CBP-associated factor/histone deacetylase 5 in the development of cardiac hypertrophy. Circ Res. 2014;114:1133–43.
66. Choubey SK, Jeyakanthan J. Molecular dynamics and quantum chemistry-based approaches to identify isoform selective HDAC2 inhibitor—a novel target to prevent Alzheimer's disease. J Recept Signal Transduct Res. 2018;38:266–78.
67. Tan Y, Delvaux E, Nolz J, Coleman PD, Chen S, Mastroeni D. Upregulation of histone deacetylase 2 in laser capture nigral microglia in Parkinson's disease. Neurobiol Aging. 2018;68:134–41.
68. Laugesen A, Helin K. Chromatin repressive complexes in stem cells, development, and cancer. Cell Stem Cell. 2014;14:735–51.
69. Guan JS, Haggarty SJ, Giacometti E, Dannenberg JH, Joseph N, Gao J, et al. HDAC2 negatively regulates memory formation and synaptic plasticity. Nature. 2009;459:55–60.
70. Gonzalez-Zuniga M, Contreras PS, Estrada LD, Chamorro D, Villagra A, Zanlungo S, et al. c-Abl stabilizes HDAC2 levels by tyrosine phosphorylation repressing neuronal gene expression in Alzheimer's disease. Mol Cell. 2014;56:163–73.
71. Maletic V, Raison C. Integrated neurobiology of bipolar disorder. Front Psychiatry. 2014;5:98.
72. de la Fuente Revenga M, Ibi D, Saunders JM, Cuddy T, Ijaz MK, Toneatti R, et al. HDAC2-dependent antipsychotic-like effects of chronic treatment with the HDAC inhibitor SAHA in mice. Neuroscience. 2018;388:102–17.
73. Limanaqi F, Biagioni F, Busceti CL, Ryskalin L, Fornai F. The effects of proteasome on baseline and methamphetamine-dependent dopamine transmission. Neurosci Biobehav Rev. 2019;102:308–17.
74. Lauridsen JB, Johansen JL, Rekling JC, Thirstrup K, Moerk A, Sager TN. Regulation of the Bcas1 and Baiap3 transcripts in the subthalamic nucleus in mice recovering from MPTP toxicity. Neurosci Res. 2011;70:269–76.
75. Ishimoto T, Ninomiya K, Inoue R, Koike M, Uchiyama Y, Mori H. Mice lacking BCAS1, a novel myelin-associated protein, display hypomyelination, schizophrenia-like abnormal behaviors, and upregulation of inflammatory genes in the brain. Glia. 2017;65:727–39.
76. You C, Savarese A, Vandegrift BJ, He D, Pandey SC, Lasek AW, et al. Ethanol acts on KCNK13 potassium channels in the ventral tegmental area to increase firing rate and modulate binge-like drinking. Neuropharmacology. 2019;144:29–36.
77. Judy JT, Zandi PP. A review of potassium channels in bipolar disorder. Front Genet. 2013;4:105.
78. Avram S, Shaposhnikov S, Buiu C, Mernea M. Chondroitin sulfate proteoglycans: structure-function relationship with implication in neural development and brain disorders. Biomed Res Int. 2014;2014:642798.
79. Ganai SA, Ramadoss M, Mahadevan V. Histone deacetylase (HDAC) inhibitors—emerging roles in neuronal memory, learning, synaptic plasticity and neural regeneration. Curr Neuropharmacol. 2016;14:55–71.
80. Yamakawa H, Cheng J, Penney J, Gao F, Rueda R, Wang J, et al. The transcription factor Sp3 cooperates with HDAC2 to regulate synaptic function and plasticity in neurons. Cell Rep. 2017;20:1319–34.
81. Kramer OH, Zhu P, Ostendorff HP, Golebiewski M, Tiefenbach J, Peters MA, et al. The histone deacetylase inhibitor valproic acid selectively induces proteasomal degradation of HDAC2. EMBO J. 2003;22:3411–20.
82. Spengler ML, Kuropatwinski KK, Comas M, Gasparian AV, Fedtsova N, Gleiberman AS, et al. Core circadian protein CLOCK is a positive regulator of NF-kappaB-mediated transcription. Proc Natl Acad Sci USA. 2012;109:E2457–65.
83. Wagner T, Kiweler N, Wolff K, Knauer SK, Brandl A, Hemmerich P, et al. Sumoylation of HDAC2 promotes NF-kappaB-dependent gene expression. Oncotarget. 2015;6:7123–35.
84. Ashburner BP, Westerheide SD, Baldwin AS Jr. The p65 (RelA) subunit of NF-kappaB interacts with the histone deacetylase (HDAC) corepressors HDAC1 and HDAC2 to negatively regulate gene expression. Mol Cell Biol. 2001;21:7065–77.
85. Howard AD, Wang R, Pong SS, Mellin TN, Strack A, Guan XM, et al. Identification of receptors for neuromedin U and its role in feeding. Nature. 2000;406:70–4.
86. Vallof D, Vestlund J, Engel JA, Jerlhag E. The anorexigenic peptide neuromedin U (NMU) attenuates amphetamine-induced locomotor stimulation, accumbal dopamine release and expression of conditioned place preference in mice. PloS ONE. 2016;11:e0154477.
87. Graham ES, Littlewood P, Turnbull Y, Mercer JG, Morgan PJ, Barrett P. Neuromedin-U is regulated by the circadian clock in the SCN of the mouse. Eur J Neurosci. 2005;21:814–9.
88. Lee IT, Chang AS, Manandhar M, Shan Y, Fan J, Izumo M, et al. Neuromedin s-producing neurons act as essential pacemakers in the suprachiasmatic nucleus to couple clock neurons and dictate circadian rhythms. Neuron. 2015;85:1086–102.

89. Harvey AG. Sleep and circadian rhythms in bipolar disorder: seeking synchrony, harmony, and regulation. Am J Psychiatry. 2008;165:820–9.
90. Landgraf D, Joiner WJ, McCarthy MJ, Kiessling S, Barandas R, Young JW, et al. The mood stabilizer valproic acid opposes the effects of dopamine on circadian rhythms. Neuropharmacology. 2016;107:262–70.
91. Gekakis N, Staknis D, Nguyen HB, Davis FC, Wilsbacher LD, King DP, et al. Role of the CLOCK protein in the mammalian circadian mechanism. Science. 1998;280:1564–9.
92. Hao Y, Creson T, Zhang L, Li P, Du F, Yuan P, et al. Mood stabilizer valproate promotes ERK pathway-dependent cortical neuronal growth and neurogenesis. J Neurosci. 2004;24: 6590–9.
93. Cui SS, Yang CP, Bowen RC, Bai O, Li XM, Jiang W, et al. Valproic acid enhances axonal regeneration and recovery of motor function after sciatic nerve axotomy in adult rats. Brain Res. 2003;975:229–36.
94. Hockly E, Richon VM, Woodman B, Smith DL, Zhou X, Rosa E, et al. Suberoylanilide hydroxamic acid, a histone deacetylase inhibitor, ameliorates motor deficits in a mouse model of Huntington's disease. Proc Natl Acad Sci USA. 2003;100:2041–6.
95. Kurita M, Holloway T, Garcia-Bea A, Kozlenkov A, Friedman AK, Moreno JL, et al. HDAC2 regulates atypical antipsychotic responses through the modulation of mGlu2 promoter activity. Nat Neurosci. 2012;15:1245–54.
96. Tsankova NM, Berton O, Renthal W, Kumar A, Neve RL, Nestler EJ. Sustained hippocampal chromatin regulation in a mouse model of depression and antidepressant action. Nat Neurosci. 2006;9:519–25.
97. Singec I, Crain AM, Hou J, Tobe BTD, Talantova M, Winquist AA, et al. Quantitative analysis of human pluripotency and neural specification by in-depth (Phospho)proteomic profiling. Stem Cell Rep. 2016;7:527–42.
98. Li W, Sun W, Zhang Y, Wei W, Ambasudhan R, Xia P, et al. Rapid induction and long-term self-renewal of primitive neural precursors from human embryonic stem cells by small molecule inhibitors. Proc Natl Acad Sci USA. 2011;108:8299–304.
99. Madison JM, Zhou F, Nigam A, Hussain A, Barker DD, Nehme R, et al. Characterization of bipolar disorder patient-specific induced pluripotent stem cells from a family reveals neurodevelopmental and mRNA expression abnormalities. Mol Psychiatry. 2015;20:703–17.
100. Maroof AM, Keros S, Tyson JA, Ying SW, Ganat YM, Merkle FT. et al. Directed differentiation and functional maturation of cortical interneurons from human embryonic stem cells. Cell Stem Cell. 2013;12:559–72.
101. Hunsberger JG, Austin DR, Chen G, Manji HK. Cellular mechanisms underlying affective resiliency: the role of glucocorticoid receptor- and mitochondrially-mediated plasticity. Brain Res. 2009;1293:76–84.
102. Kim D, Pertea G, Trapnell C, Pimentel H, Kelley R, Salzberg SL. TopHat2: accurate alignment of transcriptomes in the presence of insertions, deletions and gene fusions. Genome Biol. 2013;14:R36.
103. Anders S, Pyl PT, Huber W. HTSeq–a Python framework to work with high-throughput sequencing data. Bioinformatics. 2015;31:166–9.
104. Volk DW, Matsubara T, Li S, Sengupta EJ, Georgiev D, Minabe Y, et al. Deficits in transcriptional regulators of cortical parvalbumin neurons in schizophrenia. Am J Psychiatry. 2012;169:1082–91.
105. Pertea M, Kim D, Pertea GM, Leek JT, Salzberg SL. Transcript-level expression analysis of RNA-seq experiments with HISAT, StringTie and Ballgown. Nat Protoc. 2016;11:1650–67.
106. Fischer A, Sananbenesi F, Wang X, Dobbin M, Tsai LH. Recovery of learning and memory is associated with chromatin remodelling. Nature. 2007;447:178–82.
107. Zhang B, Horvath S. A general framework for weighted gene co-expression network analysis. Stat Appl Gen Mol Biol. 2005;4: Article17.
108. Langfelder P, Zhang B, Horvath S. Defining clusters from a hierarchical cluster tree: the Dynamic Tree Cut package for R. Bioinformatics. 2008;24:719–20.